ISSN 1560-8034, 1605-6582 (On-line), SPQEO, 2020. V. 23, N 1. P. 05-28.

Doping the thin films by using the original Close Space Sublimation method

V.S. Khomchenko*, M.V. Sopinskyy, V.A. Dan'ko, G.P. Olkhovik

V. Lashkaryov Institute of Semiconductor Physics, NAS of Ukraine
41, prospect Nauky, 03680 Kyiv, Ukraine
**E-mail: vsk@isp.kiev.ua*

Abstract. The review is devoted to the results of studies on the structure, morphology, optical and luminescent properties of thin films doped with the modified Close Space Sublimation method. Using this method, ZnO and ZnS films were doped with impurities of various metals – Ag, Cu, Ga. It has been shown that doping the films leads to an improvement in the crystal structure and radiative properties of films. When using doping with this method, cathodoluminescent screens with high luminance have been manufactured. The screens show more deep green color than C1 and C2 commercial phosphors. The luminance values at 300 K are 200 cd/m^2 for the ZnS⟨Cu,Ga⟩ film and 1100 cd/m^2 for the ZnO⟨Cu, Ga⟩ ones. At 77 K, the cathodoluminescence luminance for ZnO⟨Cu,Ga⟩ film is 3700 cd/m^2 and has not reached the limit value. Doping the ZnO with copper has greatly improved the crystal structure and made it possible to obtain films with white-light emission. Ag doping suppresses the wide visible bands of photoluminescence spectra. The intensity of ultraviolet band is 15-fold increased as compared to their reference non-doped films. The ultraviolet/visible emission ratio reached 20.

Keywords: thin films, ZnS, ZnO, Ag, Cu, Ga, doping, Close Space Sublimation.

https://doi.org/10.15407/spqeo23.01.05
PACS 68.55.-a, 68.55.J-, 68.55Ln, 78.20.-e, 81.15.Aa

Manuscript received 23.12.19; revised version received 05.02.20; accepted for publication 18.03.20; published online 23.03.20.

1. Introduction

There exists a wide variety of techniques for fabrication and doping the thin films. To avoid associated chemical disposals or keep safe from toxic or combustible gas usages in any semiconductor fabrication facilities, many researchers choose physical vapor deposition as the simplest method. One of such processes is called Close-Space Sublimation (CSS) (the notations "Closed Space Sublimation", "Close Spaced Sublimation", "Closed Spaced Sublimation", "Close Spaced Vacuum Sublimation (CSVS)", "Close-Spaced Vapor Transport (CSVT)", "Sublimation Sandwich Method" are also used), which is a kind of thermal evaporation by nature. The CSS technique is one of the most economically effective and cheap. This makes it a very viable technique for large-scale manufacturing. Films and crystals of semiconductors such as SnS [1], CdTe [2], CdS/CdTe [3] and others have been obtained using this method.

This method is based on the thermal-heating-induced sublimation of a material followed by vapor condensation onto a closely spaced substrate. The cross dimensions of the source and the substrate greatly exceed the distance between them. In "classic" CSS, the substrate to be coated and the source material are both placed in a vacuum chamber, which is pumped out, the substrate is held at some lower temperature compared to the source. As a result, the setup used for film deposition by close space sublimation is complex and includes a vacuum apparatus, a gas mixture feeding unit, and a system of heaters and controllers to control the temperatures of the evaporated material and substrate. One of the simplest schemes of this setup, which was used to evaporate CdTe films, is described in [2]. This technique can use alternate exposure to the different elemental sources.

An inexpensive and eco friendly modified method of isothermal close space sublimation at atmospheric pressure in quasi-closed volume has been suggested by Khomchenko *et al.* [4]. As a result, we were able to significantly simplify the design of the setup intended for film deposition and doping. We were the first to use this method for doping the semiconductor films with metals. The present review systemizes the results regarding the structure, morphology, optical and luminescent properties of ZnO and ZnS films CSS-doped with Ag, Cu, Ga.

© 2020, V. Lashkaryov Institute of Semiconductor Physics, National Academy of Sciences of Ukraine

2. Methods and materials

The main features of this our simplified modification of CSS method are as follows: i) the absence of vacuum chamber (which means using a non-vacuum method); ii) both doping and annealing simultaneously take place; iii) the whole system is at the same temperature.

The schematic diagram of implementation of this method is shown in Fig. 1. Sublimation of the source material was carried out in a quasi-closed silica crucible placed into a muffle furnace. The parameters that determine the mass transfer processes of the source material are the temperature of crucible, source-substrate distance and composition of the gas medium inside the source-substrate sandwich. The gaseous medium required for the film deposition or doping was formed by selecting a suitable powder mixture fill for the silica crucible holding the "source-substrate" sandwich. The presence of oxygen sorbents in the powder together with the reduced gas exchange rate in the quasi-closed silica crucible made it possible to reduce the partial pressure of oxygen, as a consequence, reducing the oxidation rate of the substance under sublimation.

In the case of doping the semiconductors with metals, the latter are introduced into the semiconductor film through the vapor condensation on the film surface and subsequent diffusion into the film bulk when heating them in a furnace. This method [4] allows controlling the concentration of the doping elements by changing the furnace temperature, since there is a correlation between the metal vapor pressure of the doping element in the film and the CSS doping temperature T_d. The doping temperature T_d varied within 500…800 °C in dependence on the type of metal. Initial zinc oxide and zinc sulfide films were obtained by different methods such as electron-beam evaporation, reactive rf-magnetron sputtering, and pyrolysis of organometallic compounds (MOCVD technique). We used glass, ceramic, silicon, Si/SiO_2, Si/SiN_x and sapphire substrates.

X-ray diffraction (XRD) measurements were performed by DRON-3M X-ray diffractometer operating with CuK_α radiation (λ = 0.1541 nm). The morphological properties of films were studied using NanoScope IIIa Dimension 3000 atomic force microscope (AFM). To provide high lateral resolution and sensitivity, the tapping mode of measurements was applied. Measurements were performed using commercial silicon tips NSG-11 (NT-MDT, Russia) with the nominal tip apex radius of 10 nm. Photoluminescence (PL) spectra were excited by pulsed nitrogen laser (337 nm) and measured at room temperature. The PL spectra were recorded using Horiba JobinYvon T64000 spectrometer. The cathodoluminescence (CL) signal was detected using an Oxford Instruments MonoCL2 system in Philips XL30 SEM at the electron energy in the beam of 15 keV. All the measurements were performed at room temperature.

CL characteristics were measured in the demountable cathode ray tube with a variable beam current from 0 to 50 μA. The phosphor screen samples were excited by electron beam at the accelerating voltage 50 kV over a 2.8×2.1 cm^2 area scanned. The standard television raster was formed on the screen plane (at 15.625 kHz horizontal and 50 Hz vertical scanning frequencies). The effective ionization depth for electrons equals 4.15 μm for ZnS film and 2.85 μm for ZnO film at the accelerating voltage 50 kV.

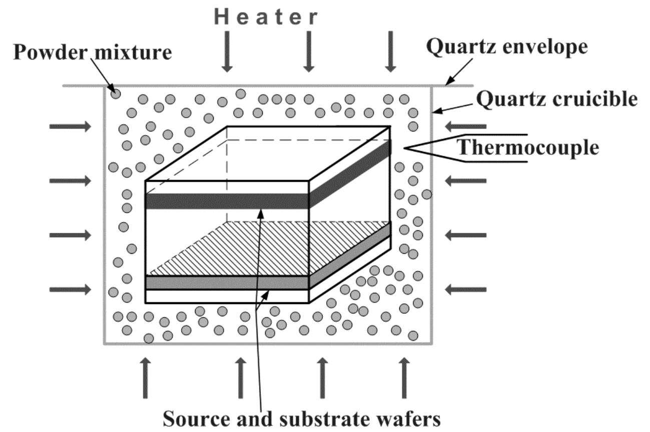

Fig. 1. Schematic diagram of CSS method.

3. ZnS, ZnO films doped with Cu, Ga

3a. Electroluminescent display device based on ZnS⟨Cu,Ga⟩ films

The ZnS, ZnS⟨Cu⟩ films were prepared by physical (electron-beam evaporation (EBE)) and chemical (MOCVD) methods. Ga-doping was realized using the CSS method via annealing of ZnS⟨Cu⟩ films at 800…900 °C with Ga vapors. Thin film electroluminescent devices (TFELDs) were made on both glass and ceramic substrates. TFELDs had a conventional double (or single) insulating structure: MISIM or MSIM (M – electrode, I – insulator, S – semiconductor). For glass substrates, back transparent ITO film and upper Al film were used as electrodes. Al_2O_3 film was used as insulator (I). The Al_2O_3 thickness was 20…300 nm, and the ZnS film (S) thickness was 0.6…2 μm. The devices on the ceramic substrates had a metal back electrode and a $BaTiO_3$ thick insulator sheet (~ 40 μm) formed on the substrate. A semitransparent Al upper electrode was formed by means of thermal evaporation. The ZnS⟨Cu⟩ films thickness was 0.6 μm. The schematic diagram of the structure is shown in Fig. 2.

XRD patterns reveals a cubic structure of ZnS film (high and intense peak at 2θ = 28.5°) with preferred orientation along ⟨111⟩ direction (Fig. 3). Annealing (both without and with gallium vapors) does not transform the type of the films structure. It must be emphasized that ZnO phase was not detected. In the films after annealing with Ga co-doping, a deviation from stoichiometric ZnS compound was not also detected using the energy-dispersion microprobe analysis at the measurement accuracy 0.05 at.% [5].

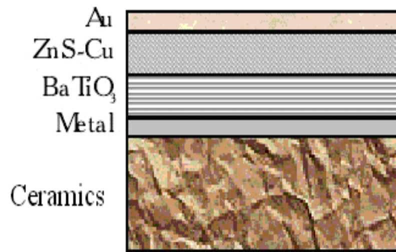

Fig. 2. Schematic diagram of fabricated TFEL devices.

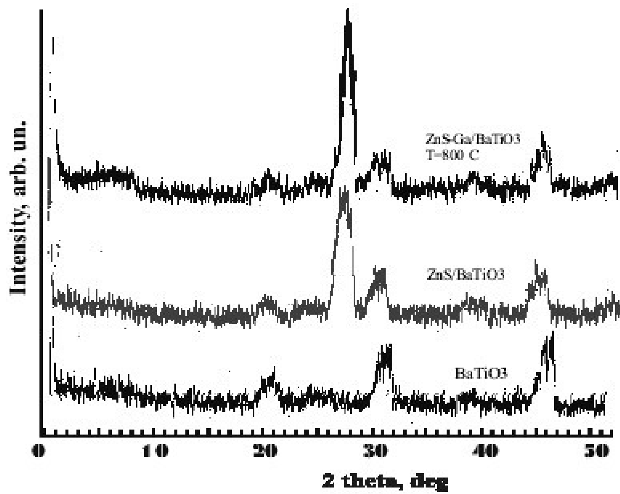

Fig. 3. X-ray diffraction patterns of clear $BaTiO_3$ substrate and $ZnS/BaTiO_3$ structures (as-deposited and annealed at 850 °C).

A surface of $ZnS/BaTiO_3$ structures was examined by atomic force microscopy. It was detected that $BaTiO_3$ substrate consists of large 7…9 µm grains and remains unchangeable over all treatments. After depositing ZnS, these grains have been covered with small subgrains. Fig. 4 presents the changes of ZnS film after annealing at 800 °C and annealing with Ga. In the initial state (Fig. 4a), the ZnS film consists of small size (200…400 nm) grains that are not clearly separated. After annealing, the grains coalesce. We can observe more large blocks (~ 600 nm) separated by deep boundaries (Fig. 4b). Besides, the small subgrains remain in the block area but all of them are grown together. After annealing at 800 °C with the Ga presence, the blocks get larger (~750 nm) and clearly separated. They become smoothed, and no subgrains are observed.

It was revealed [6] that Ga and Cl act not only as co-dopant for improvement of luminescent properties, but also as a promotor of collecting and secondary recrystallization processes, which facilitate a coarse-grain formation.

Diffusing Ga atoms inside the film gather at subgrain boundaries and accelerate the grain growth process, when large grains grow at the cost of small ones with decreasing surface energy [7]. Presence of some liquid phase (in our case Ga with its melting point 29.7 °C) essentially accelerates all mass-transfer processes during annealing, and as a consequence, the intense magnification of grain sizes occurs. Doping the ZnS film with copper and chlorine during the annealing process reduces the phase transition temperature – from 1020 down to 800 °C [8]. The transition of ZnS film sphalerite lattice to wurtzite results in the displacement of the blue emission band towards the short-wave range by 0.07 eV [6]. It is known that the sphalerite structure predominates when the bonding is predominantly covalent, whereas the more ionic systems favor the wurtzite form [8]. As Cu^+ cations occupy the zinc sublattice, the incorporation of $Ga^{3+}(Al^{3+})$ trivalent cations in the same sublattice does not reduce the covalent binding. While incorporation of Cl^- anions in sulphur sublattice with Cu^+ cations in zinc sublattice changes the binding in the ZnS lattice to the more ionic one. In ZnS⟨Cu,Cl,Ga⟩ films [9], the amount of Cu^+ and Cl^- ions diffused into ZnS lattice from ZnS⟨Cu,Cl⟩ powder during thermodiffusion is the same, but a part of ions can be gathered at the dislocations, subgrain and grain boundaries. The additional Ga doping by using the CSS method leads to smooth grains with the largest grain size, which, in its turn, results in more homogeneous distribution of Cu^+ and Cl^- in sublattices and, hereby, increases the amount of Cu^+–Cl^- ionic binding, which affects the phase transition temperature.

Photoluminescence (PL) and electroluminescence (EL) properties of ZnS⟨Cu⟩ films strongly depend on the copper concentration and film thickness [10]. But these properties are even more dependent on Ga doping-annealing. So, PL and EL are not observed when the Cu content in the ZnS⟨Cu⟩ target was 0.5 wt.% and the ZnS⟨Cu⟩ film thickness was 500 nm. When the film thickness is increased up to 1 µm, a very poor PL appears. It was increased five-fold as much, when the films were annealed at 850 °C. The PL intensity was increased to the factor of 100, when the ZnS⟨Cu⟩ films were doped with Ga via annealing of ZnS⟨Cu⟩ films at 850 °C with the presence of Ga vapor. The PL spectra of the films are shown in Fig. 5. Photoluminescence of as-deposited ZnS⟨Cu⟩ films has peaks at 410…420 nm, and, most importantly, its bandwidth is very narrow (~50 nm) [10], even more narrow than that of ZnS⟨Cu⟩ nanocrystals with the 70-nm size [11]. Let's mark that we observed the spectra with fine structure lines on the high energy side of the blue band. Distance between peaks of the lines is 0.12 eV.

The annealing in Ga vapors causes changes in the spectrum. The blue band peak shifts to λ = 450 nm, the green band at λ = 520 nm is displayed. The emission maximum positions are characteristic for ZnS⟨Cu⟩ crystals. This spectra modification corresponds with growth of the grain size up to 750 nm. The view of spectra depends on the ratio of Cu and Ga concentrations [12]. Four emission bands are presented in the PL spectra – blue (at 450 nm), green (at 520 nm), yellow (at 585 nm) and red (at 650 nm). The latter two bands are characteristic for Ga doping.

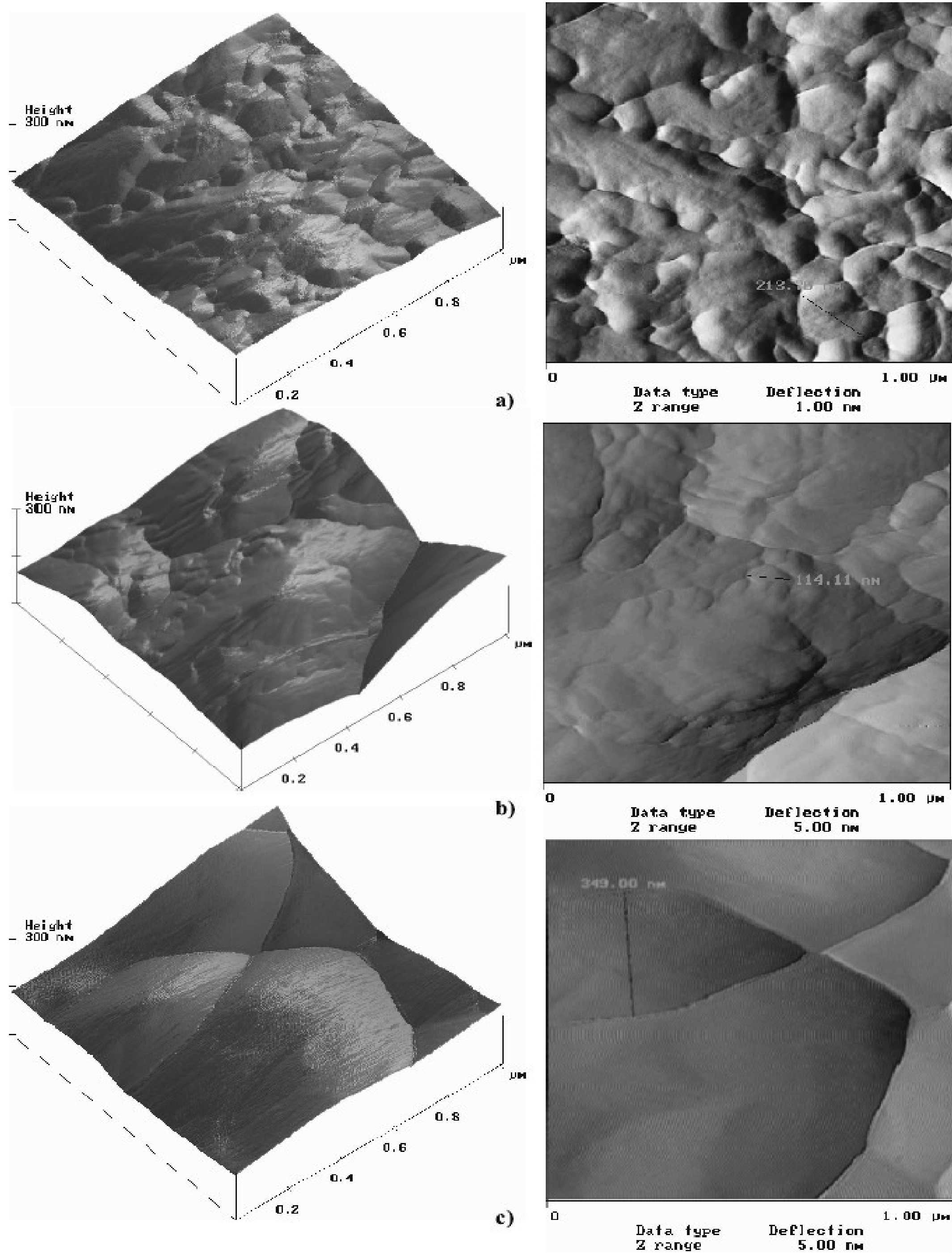

Fig. 4. Height 3D (on the left) and deflection (on the right) AFM images of the ZnS EL films surfaces: (a) initial state, (b) annealed at 800 °C, (c) annealed at 800 °C with Ga presence.

The red band isn't observed in EL spectra. The highest luminance is received for the green and yellow bands – 800 cd/m^2 at 5 kHz. The luminance 30 cd/m^2 is obtained for the blue band. As shown in Fig. 6, the EL properties are changed via thermal treatment in the following manner. In the devices with ZnS⟨Cu⟩ films annealed at 850 °C, the luminance is just three times higher than that in the devices with as-deposited ZnS⟨Cu⟩ films. However, when the films are annealed at 850 °C, ZnS⟨Cu⟩ devices with Ga doping started to show rapid increase in the luminance and shift of the threshold voltage from 110 to 10 V. The luminance of EL is increased up to the factor 10 for the blue color emission films and 100 – for the green (yellow) color emission films.

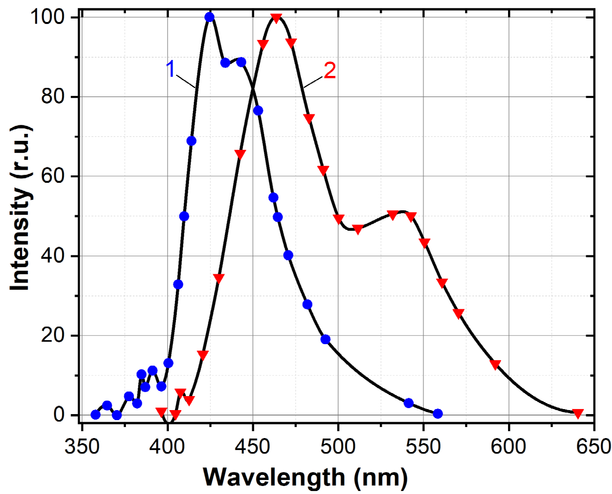

Fig. 5. Photoluminescence spectra of ZnS⟨Cu⟩ films: as-grown (*1*) and after Ga doping-annealing at 850 °C (*2*).

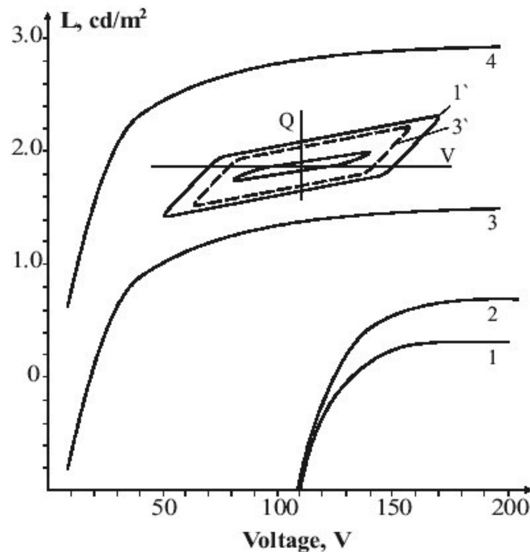

Fig. 6. Voltage dependences of luminance (*1–4*) and transferred charge (*1′*, *3′*) under 1 kHz sine wave of ZnS⟨Cu⟩ devices: as-grown (*1*, *1′*), after annealing at 850 °C (*2*), after doping-annealing at 850 °C (*3*, *3′* – blue, *4* – green and yellow color emission).

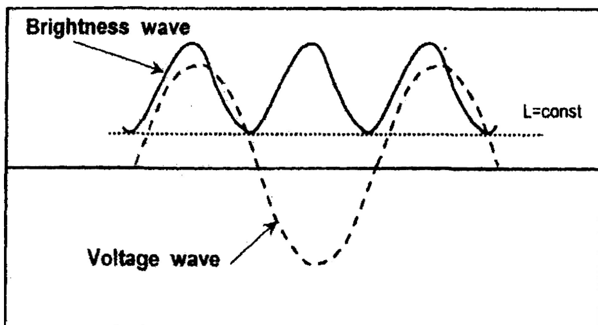

Fig. 7. Brightness wave of the ZnS⟨Cu⟩ first type layer with blue color at 500 Hz.

Charge-voltage (*Q–V*) measurements showed a significant transferred charge presented in the devices with non-annealed ZnS⟨Cu⟩ films. The charge decreases gradually with annealing temperature, it is especially pronounced in Ga-doped devices annealed at high temperatures. From AFM analysis and EL data [13–16], we can conclude that a significant amount of structure defects (more than likely grain boundaries) exists in the as-deposited ZnS⟨Cu⟩ films. With the grain size as large as 750 nm, the crystalline quality is significantly better than those for as-deposited or annealed films without Ga-doping. The crystalline quality improvement may increase an electron's mean free path. EL starts at the field strength $2\cdot10^6$ V·cm^{-1} (as-deposited, annealed film non-doped with Ga) which is high enough to accelerate free carriers with a mean free path $\lambda \sim 10^{-7}$ cm. For ZnS⟨Cu,Ga⟩ films, EL starts at the field strength of $2\cdot10^5$ V·cm^{-1}. In such a case, the condition for free carrier acceleration will be satisfied for $\lambda \sim 10^{-6}$ cm. The λ-value close to 10^{-6} cm was obtained earlier for ZnS⟨Cu,Cl⟩ films [17] in close agreement with the λ-value reported for the analogous powder phosphors [18].

The knowledge of EL mechanism is necessary for the film that can be considered as a potential candidate for the thin-film EL displays. The study was performed with different EL structures [19]. The films studied may be divided into the two types [20]. These types are differentiated by uniform and non-uniform distribution of the electric field in the film. The layers of first types were characterized by uniform electric field distribution. They were observed, if the MISIM structure was used. The ZnS⟨Cu⟩ thickness was about 0.6 µm, the insulator thickness ≥0.6 µm. Such a type of the layer has the electrical capacitance equal to the "geometric" one of S-layer. It is independent of the voltage, frequency and temperature.

The second type is the layer with non-uniform electric field distribution due to the contact barriers and charge polarization. These layers were obtained under the following conditions. The MSM or MSIM type structures were prepared. SnO_2 and Al were used as electrodes (M). The thickness ZnS⟨Cu⟩ (S) layer was 2…3 µm. The thickness of insulating (I) SiO layer was 0.01…0.05 µm. This layer was displaced between ZnS and Al only. It was impossible to describe the capacitance of this type layer with the expression $C = \varepsilon S/4\pi d$. Its capacity depended on the frequency, voltage, and temperature like to the Schottky barrier with deep centers [21].

The EL properties of the structure on the basis of the first type films are very similar to those for the ZnS⟨Mn⟩ MISIM structure. The voltage dependence of luminance (*L*) and transferred charge (*Q*) are shown in Fig. 6 for ZnS⟨Cu⟩ devices with blue, green and yellow color emission. Their shape is typical for the MISIM structure. The sine wave excited brightness waves is shown in Fig. 7 for blue color TFELD. It is seen that the maximum brightness corresponds to the voltage maximum. It is characteristic for an undelayed recombination

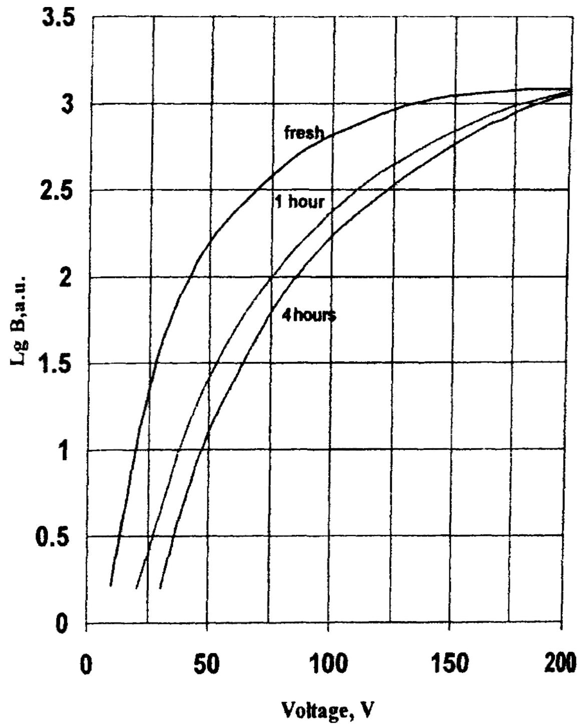

Fig. 8. Aging characteristics of ZnS⟨Cu⟩ first type layer device with blue color emission driven at 1 kHz pulse voltage, the pulse width is equal to 5 μs.

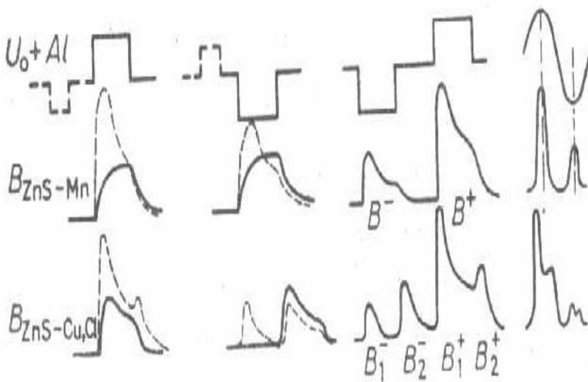

Fig. 9. Brightness waves of the ZnS⟨Cu⟩ second type films, ZnS⟨Mn⟩ films and the excitation pulse shape.

mechanism. The degradation characteristic is shown in Fig. 8 for TFELD with blue color emission. $L(V)$ dependence is shifted to the higher voltage in the first hour of operation. In the subsequent hours of operation, the shift value is decreased [20]. The emission degradation character is similar to that observed for the activator with intraionic emission mechanism (ZnS⟨Mn⟩, ZnS⟨Tb⟩). Analysis of the obtained results enables to draw conclusions that for the first type films the impact ionization model is appropriate and the mechanism of emission is an undelayed recombination.

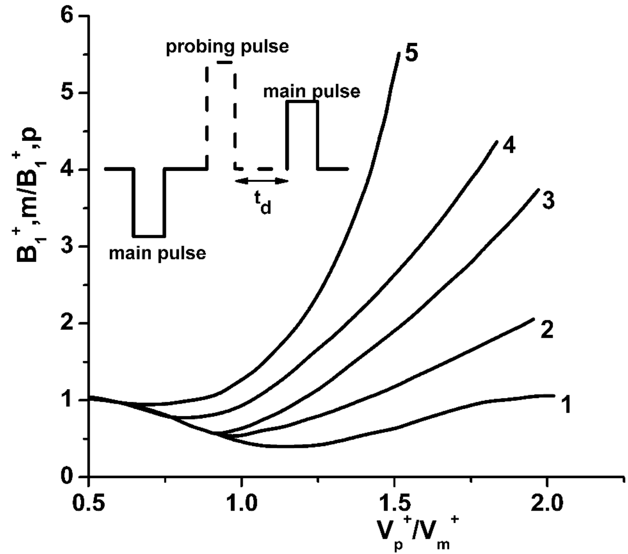

Fig. 10. Dependence of the ratio B_1^+ (at presence of probing pulse) to $B_{1,m}^+$ (without the probing pulse) on the ratio of the amplitudes of the probing and main pulses. Amplitude of main pulse is equal to 20 V, the delay time t_d between the probing and main pulse, ms: 0.2 (*1*), 0.4 (*2*), 1 (*3*), 5 (*4*). Curve *5*: amplitude of main pulse is 13 V, $t_d = 5$ ms.

The brightness waves of the second type films are similar with those for powder phosphors and differ from those of ZnS⟨Mn⟩ films (Fig. 9). Electroluminescence starts at much smaller average field strength than for the ZnS⟨Mn⟩ ones. The $L(V)$ relation is 5 times steeper for ZnS⟨Cu⟩ films than for ZnS⟨Mn⟩ ones. The following luminance equation is valid over 7 decades of brightness: $L = L_0 \cdot \exp(-b/V)$. But all experimental facts concerning the electroluminescence of second type ZnS⟨Cu⟩ films can be explained by the supposition of the impact ionization mechanism, a local field enhancement near the SnO_2 electrode and ionization of the activator centers. The relatively low average field strength at which EL starts might be explained by the field enhancement localized in the Mott–Schottky barrier. The barrier width is less than the film thickness by a factor of 3…5. If the average field strength is $3 \cdot 10^4$ V/cm, the barrier field is approximately 10^5 V/cm. The condition for free carrier acceleration will be satisfied for a mean free path of $\lambda > 10^{-7}$ cm. For ZnS⟨Cu⟩, the λ-value is equal to 10^{-6} cm [17]. For appearance of two brightness peaks during each half-cycle of the exciting voltage (Fig. 9), two explanations are offered: delayed recombination mechanism and a direct excitation by the polarization field existing after switching-off the external voltage.

It has been investigated whether the primary brightness peak B_1^+ is due to recombination centers excited during this voltage pulse (undelayed recombination) or whether the supposition of a delayed recombination is correct. One fact confirming undelayed character recombination is the observed influence of a positive probing pulse on the brightness peak B_1^+ [17].

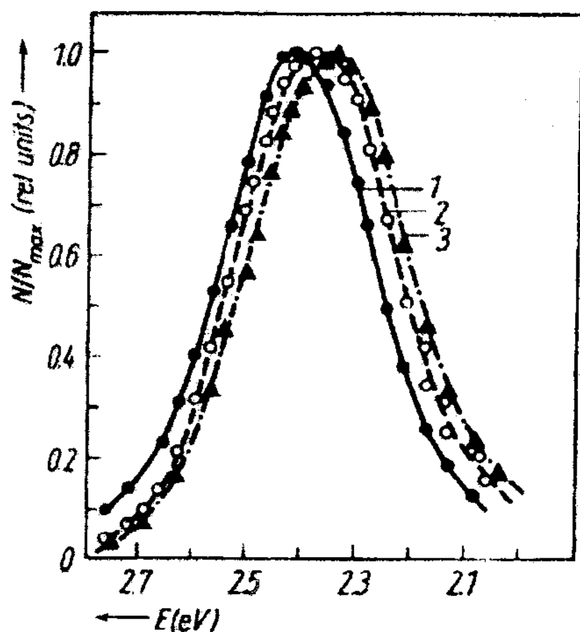

Fig. 11. EL spectra of ZnS:Cu second type films under different excitation voltages at 200 K; the frequency is 2 kHz, the film thickness is 2 μm; *1*, *2*, *3* – 30, 45 and 60 V RMS values, respectively. *N* – photon number.

The dependence of the ratio B_1^+ (at the presence of probing pulse) to $B_{1,m}^+$ (at the absence of probing pulse) on the ratio of amplitudes of the probing and main pulses is shown in Fig. 10. According to Fig. 10, the delay time t_d between the probing pulse and the main one as well as their amplitude relation show a double effect on B_1^+. At decreasing t_d, the peak B_1^+ decreases (for $t_d < 0.2$ ms, see curve *1*). The peak B_1^+ increases when t_d is long and $V_p/V_m > 1$ (see curves *2*–*5*). The diminution of B_1^+ by probing pulse may be explained as follows. After the probing pulse, a polarizing field is present in the layer, the polarity of which is opposite to that of the main voltage pulse, thus the internal field is reduced during the main pulse. The polarization field relaxes rapidly as seen from the time dependence of the effect (only small t_d values are effective). If the time t_d is large, the polarization field due to the probing pulse diminishes considerably before the main pulse starts. In this case, when increasing V_p, B_1^+ increases. This may be explained as follows. A higher probing pulse produces more excited centers, a fraction of which is still excited at the start of the main pulse. The additional number of excited centers will relatively increase with decreasing V_m and increasing V_p^+/V_m^+ in accordance with experiments. The effects of decreasing B_1^+ prevail at small t_d, although the polarization field is small, too, thus the brightness B_1^+ is determined by the number of excited centers during the main pulse [17].

The additional argument was obtained from investigation of EL spectra that confirm undelayed recombination. The strong electrical field results in some long-wave shift of ZnS⟨Cu,Cl⟩ green band due to the Franz–Keldysh effect [22–24] (see Fig. 11). The fact that the Franz–Keldysh shift of the emission band takes place indicates that the recombination occurs in the region of intense electric field. It should be noted that in powder phosphors of the same composition, on the contrary, a "delayed" recombination takes place. Such a difference between the electroluminescence of the powder and the film samples may be explained taking into account that in the films electrons are continuously injected from the electrodes, whereas in powder phosphors with dielectric matrix the continuous current of carriers is very weak.

The second type ZnS⟨Cu⟩ films degradation is very fast process. Deterioration of the EL device characteristics is due to the drift of defects charge followed by widening of a space charge region and by the change of the center concentration in the high field region.

Thus, the evidence is presented that ZnS⟨Cu⟩ film EL mechanism is direct impact excitation (ionization) of luminescent centers by hot electrons, and the emission mechanism is an undelayed recombination. The fast deterioration of the EL device characteristics is observed in second-type ZnS⟨Cu⟩ films. The ZnS⟨Cu⟩ TFELD stability may be increased by means of choice of correct EL layer type.

3b. Cathodoluminescent properties of the ZnS and ZnO thin films doped with Cu, Ga [25–28]

The initial films under investigation have been prepared by EBE evaporation from a ZnS⟨Cu⟩ target on a monocrystalline sapphire substrate with further special new processing. Under evaporation, the substrate was heated to 150…200 °C, the film thickness was 9 μm. Cu concentration in target was varied from 0.06 to 0.12 wt.%. Parameters of these film phosphors were significantly modified by using special non-vacuum CCS high-temperature (700…800 °C) annealing/treatment of ZnS⟨Cu⟩ film in suitable (S_2- or O_2-riched) atmosphere. For Cu charge compensation, the films were doped with Ga from the Ga melt during film annealing [4]. Such a method of doping was first used for CL films. The Al layer with 0.1 μm thickness was evaporated directly onto the phosphor films after annealing.

The crystalline structure and morphology of the obtained films were investigated by X-ray diffraction technique (Cu K_α radiation) and atomic force microscopy. PL measurements were carried out with the excitation source of a nitrogen laser (λ = 337 nm). When measuring luminescence the 9 μm phosphor film thickness provides favourable conditions for the transfer of effective energy from the exciting electron beam to the phosphor and the excitation of the film deep uniform regions far removed from the both film interfaces.

The analysis of XRD patterns shows that all as-deposited films were ZnS⟨Cu⟩ with the sphalerite crystal structure and preferred orientation in ⟨111⟩ direction (Fig. 12, curve *1*). Annealing in S_2-rich atmosphere does not transform the type of ZnS⟨Cu⟩ film crystal structure (both without and with gallium vapor) [25].

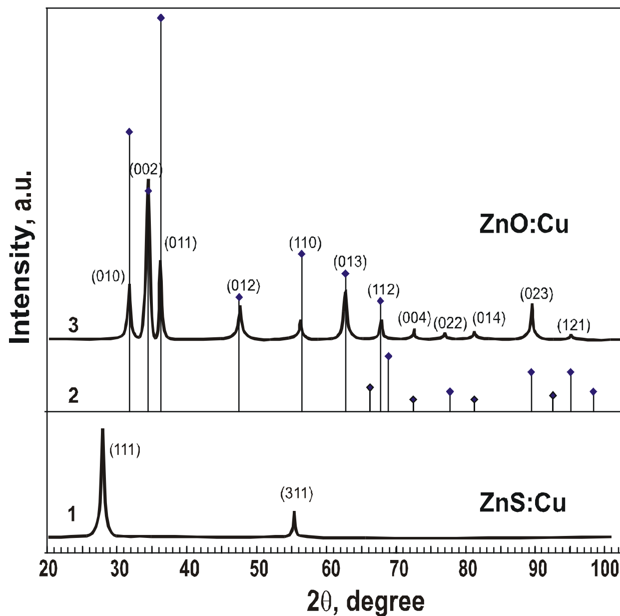

Fig. 12. X-ray diffraction patterns of ZnS⟨Cu⟩ (*1*) and ZnO⟨Cu⟩ (*3*) films on sapphire substrate and the stimulated pattern for ZnO powder (*2*).

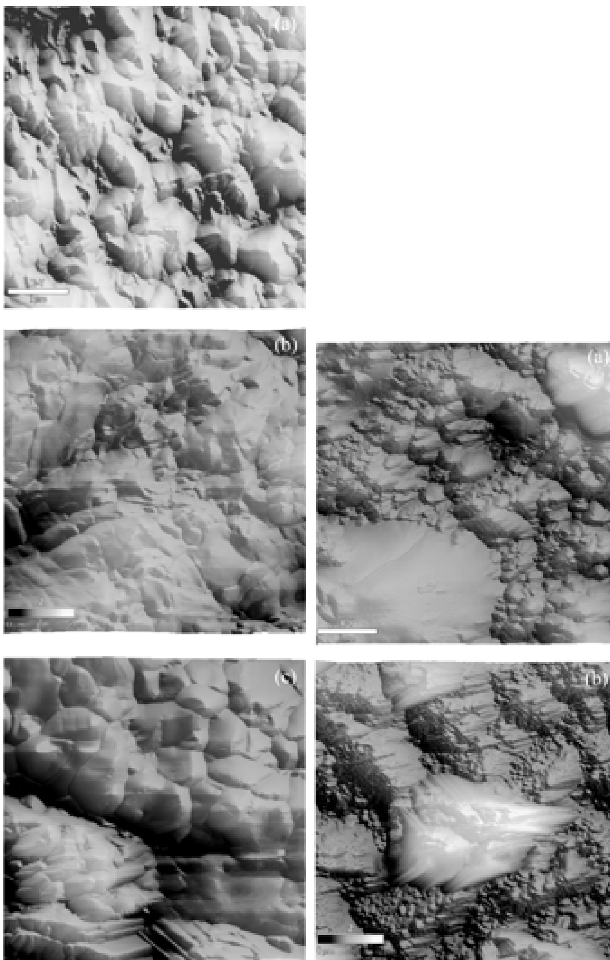

Fig. 13. AFM images of surface morphology of ZnS⟨Cu⟩ films (left column) and ZnO⟨Cu⟩ films (right column).

The XRD patterns of the ZnS⟨Cu⟩ film obtained in the result of ZnS⟨Cu⟩ film annealing in O_2-rich atmosphere as well as simulated pattern of powder ZnO are also shown in Fig. 12 (curves *3* and *2*). From a comparison of intensities of simulated data for powder ZnO and experimental data for the ZnO⟨Cu⟩ films, it can be concluded that ZnO⟨Cu⟩ films have wurtzite crystal structure with a preferred ⟨001⟩ orientation. The type of the ZnO⟨Cu⟩ film crystal structure does not change at the film annealing with Ga doping.

AFM data illustrate the role of thermal treatment and Ga doping in the crystalline structure formation process (Fig. 13). The surface morphology images of ZnS⟨Cu⟩ films are represented in Fig. 13 for an as-deposited film (a), after annealing in S_2-rich atmosphere (b) and after annealing with Ga doping at the same atmosphere, temperature and duration (c). As it can be seen, the annealing in S_2-rich atmosphere leads only to the increase in the grain mean size from 150…300 nm up to 750 nm. However, the grain boundaries remain weekly denominated and grain size distribution is non-uniform. The annealing with Ga doping results in occurence of sharp distinct grain boundaries and considerable increase in the grain size up to 950 nm.

The special thermal treatment of ZnS⟨Cu⟩ films in O_2-rich atmosphere, where transformation from ZnS to ZnO takes place, causes more pronounced change in the grain configuration. The image of AFM film morphology for this case is represented in Fig. 13a (right column). It is seen that the ZnO⟨Cu⟩ film surface is now very inhomogeneous. The polycrystalline aggregations with the grain size from 350 to 500 nm dominate, although large (about 2000 nm) formations are also observed. After the treatment in Ga vapors, the ZnO⟨Cu⟩ film surface consists of large blocks about 1200 nm in size (Fig. 13b, right column). Besides, more large formations (from 1500 to 3000 nm) are present. On the surface of main blocks, the small (about 80 nm) grains are screen as well. Since these small grains are observed in ZnO films annealed both with and without Ga vapor, they seem to be the minor product of reaction between ZnS and some contaminations from oxygen atmosphere.

As-deposited samples did not show an initial photoluminescence. Annealed films show PL in the green spectral region. ZnS⟨Cu⟩ and ZnS⟨Cu,Ga⟩ films emitted green light under UV radiation. The emission maximum is located at 520 nm. The PL and CL spectra are practically identical. From the investigation of decay curves, we determined that the 1/10 afterglow decay time is 0.6 ms. The CL spectra of ZnS⟨Cu,Ga⟩ films at different values of current density j are shown in Fig. 14. The maximum of emission is located at 530 nm. At about three-fold increasing the excitation level (average current density), the shape of emission band changed slightly, except for the region $\lambda > 600$ nm where the emission intensity was significantly decreased.

The CL spectra of ZnO⟨Cu⟩ and ZnO⟨Cu,Ga⟩ film at different excitation levels and temperatures were studied. The emission band shape for ZnO⟨Cu⟩ films is

stable at four-fold increase in the excitation level. When the temperature was decreased to 77 K, the full width at the half maximum (FWHM) decreased only slightly. CIE coordinates of ZnO⟨Cu⟩ films are $x = 0.21$, $y = 0.54$. The films show more deep green color than C1 and C2 commercial phosphors. CL luminance of ZnO⟨Cu⟩ and ZnS⟨Cu⟩ films in television raster as a function of screen excitation current density for temperatures 300 and 77 K is shown in Fig. 15. The luminance values at 300 K are 200 cd/m^2 for ZnS⟨Cu,Ga⟩ film and 1100 cd/m^2 for ZnO⟨Cu,Ga⟩ one. At 77 K the CL luminance for ZnO⟨Cu,Ga⟩ film is 3700 cd/m^2 and has not reached the limit value and can be improved using technology optimization. It indicates a considerable reserve of luminance increasing for screens based on ZnO films. Horizontal scanning frequency of an electron beam on the screen must be increased with application of heat sink to realize this reserve. The obtained results (high luminance, color coordinates values, emission band stability) point to the perspective application of ZnO⟨Cu⟩ films for projection TV and HDTV.

3c. Luminescent properties of ZnO⟨Cu⟩ films [25, 36, 40, 42]

ZnO is a wide- and direct-band gap semiconductor (3.37 eV), which room-temperature photoluminescence is of the greatest importance. The ZnO has various luminescent transitions, since different preparation techniques lead to varying structures and surface properties of ZnO. Generally, ZnO exibits two kinds of emissions: the former is the excitonic ultraviolet (UV) one at 370...380 nm and the latter is visible (VS) emission with its peak at 510...530 nm [29]. Many studies have attempted to improve the properties of ZnO by doping with transition metals such as Al [30], Mg [31], In [32], and Cu [25, 33, 34]. Among them, copper is a most preferable dopant, since ionic radii of Cu^{2+} (0.073 nm) and Zn^{2+} (0.074 nm) are similar [35], and it relatively easy replaces zinc in the lattice forming a complex with neigbor oxygen ions. Cu can interact with intrinsic defects of ZnO resulting in formation of different defect complexes which effect optical transitions in ZnO. It was found that this allows changing the emission color from green to white [36]. Cu-doped ZnO has shown an essential improvement in electrical, optical, magnetic and luminescent performances [37]. Different techniques are used to grow ZnO⟨Cu⟩ films, namely: pulsed laser deposition [38], magnetron sputtering [39], metal-organic chemical vapour deposition under atmospheric pressure [40]. Cu can be added to ZnO films during the growth process [25, 34, 36, 40] or copper impurity can be introduced into the already deposited ZnO film [41, 42] by different techniques. We investigated the effect of Cu doping by using the CSS technique on structure and luminescent properties of ZnO thin films [42]. The isothermal CSS process [4] has been used for doping the ZnO films with Cu under the atmospheric pressure. The obtained ZnO⟨Cu⟩ films were heated in humid air.

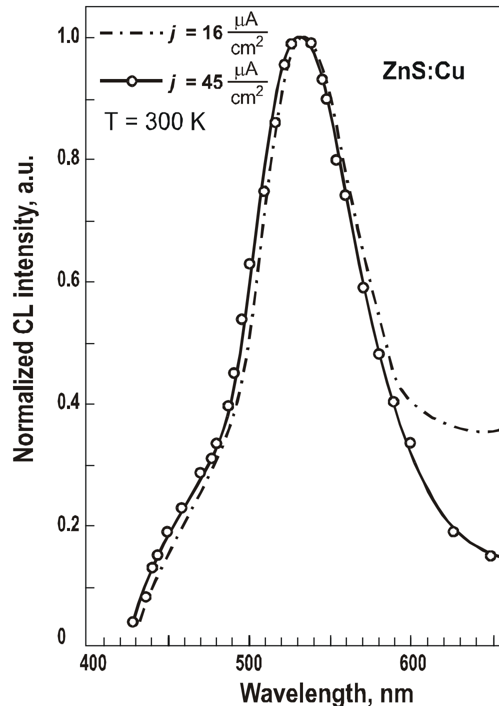

Fig. 14. Cathodoluminescence spectra for ZnS⟨Cu⟩ film at the temperature 300 K for two excitation levels (average current densities *j*).

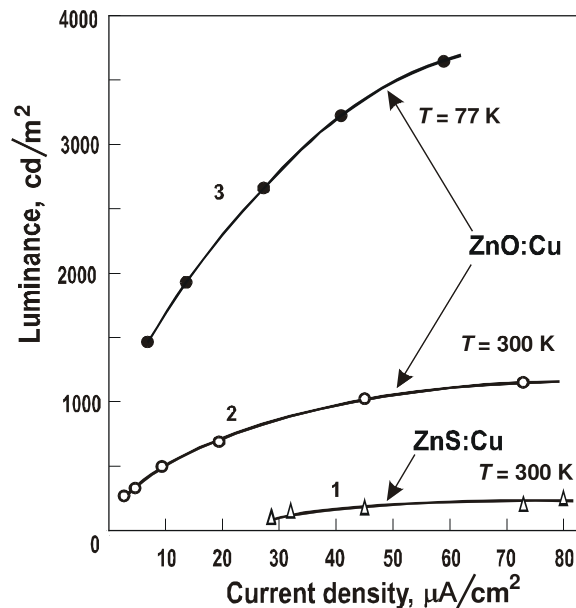

Fig. 15. Cathodoluminescence luminance of ZnS⟨Cu⟩ (*1*) and ZnO⟨Cu⟩ (*2*, *3*) films as a function of current density at the temperatures 300 and 77 K.

Beneficial effect of water vapor on growth of ZnO crystals and on structural properties of ZnO films is well known for a long time [43, 44, 45]. This method represents favorable conditions at appropriate temperature for the impurity to be effectively introduced into ZnO film.

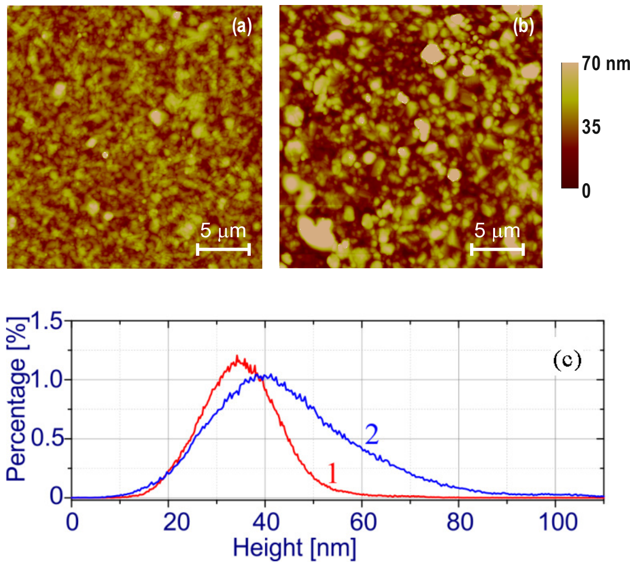

Fig. 16. AFM images of ZnO reference (a) and Cu-doped (b) ZnO films deposited on Si substrate. Surface height histograms (c) for the corresponding films (*1*, *2*).

ZnO films (approximately 0.5 μm) were deposited by radio-frequency magnetron sputtering the Zn target in vacuum chamber onto silicon and sapphire substrates. The ZnO films were deposited at the substrate temperature T_s = 150 °C. The 10-nm buffer layer SiN_x was introduced to accommodate lattice mismatch between ZnO and Si. The mismatch of lattice constants (15%) and thermal expansion coefficients (56%) between ZnO and Si are quite large. SiN_x has a relatively small lattice mismatch (5%) and thermal expansion coefficient. The deposition of films was carried out using the layer-by-layer method that was detailed in [39].

Cu doping the ZnO films was performed using the CSS process at atmospheric pressure for 1 h. A copper block was used as Cu source and $ZnO/SiN_x/Si$ and $ZnO/\alpha\text{-}Al_2O_3$ films were used as a substrate. The Cu source and the substrate were separated by a ceramic spacer with the thickness 1 mm. Cu was introduced into ZnO by condensation of their vapor on the film surface at the temperatures 500…600 °C. The doping method is based on the process of impurity diffusion through the surface of the film under heating. This method allows correlating the concentration of the doping elements by changing the temperature in the furnace. We have found that noticeable changes of luminescence spectra start at the temperatures higher than 500 °C. The doping temperature varied within 500…700 °C. The Cu vapor pressure was within $10^{-9}…10^{-4}$ Pa [46]. We used three doping levels. The low level of doping corresponds to $1.33\cdot10^{-9}$ Pa, the mediate – to $1.33\cdot10^{-7}$ Pa, and the high – to $7\cdot10^{-5}$ Pa. After the CSS processing, these ZnO⟨Cu⟩ films were annealed at the temperature 600 °C in wet medium for 1 hour (the density of water vapors was about 0.08 g/m^3). Beside ZnO⟨Cu⟩ films, ZnO reference films were treated at the same conditions in order to separate the effects of the temperature annealing on the properties of films.

Another type ZnO⟨Cu⟩ films were deposited by EBE from ZnO⟨Cu⟩ target onto sapphire substrates. The Cu concentration in the target was from 0.06 to 0.25 wt.%. The substrate was heated up to 150 °C, and the film thickness was 0.6 μm. These ZnO⟨Cu⟩ films were also annealed at the temperature 600 °C in wet media for 1 hour (the density of water vapors was close to 0.08 g/m^3).

XRD measurements showed that all ZnO films have the polycrystalline hexagonal structure. The films consist of grains with the strongly preferred (002) orientation. Doping with a small amount of copper does not change the texture of the ZnO film. Surface morphology modification caused by the doping process was investigated using AFM, since introduction of the Cu impurity by using the CSS methods is based on diffusion of Cu ions into the films through the grains or grain boundaries. Fig. 16 illustrates the effect of doping on morphology of film surface at the mediate doping level. The surface of reference ZnO film (Fig. 16a) shows complex nano-granular structure. The smallest grains (diameters of 15…20 nm) were aggregated into elongated clusters (typically 360×60 nm). Clusters were randomly oriented and separated with the depressions of 10…15 nm in depth. Surface morphology transforms drastically at Cu doping (Fig. 16b). Many elongated clusters transforms into faceted pyramidal grains. The size of their long axis ranged within 300…450 nm. The size of a small fraction of grains increased up to 60…120 nm. The depth of depressions between grains enlarged to 25…50 nm. From the statistical viewpoint, surface transformation at doping could be illustrated with height histograms. Height distributions for ZnO (curve *1*) and ZnO⟨Cu⟩ (curve *2*) films are shown in Fig. 16c. Significant widening of the surface height takes place for doped films. Corresponding RMS values are equal to 9 and 17 nm for initial and Cu-doped films.

PL emission was excited by a He-Cd laser (λ_{exc} = 325 nm, power 25 mW). The PL spectra were recorded with using the Horiba Jobin Yvon T64000 spectrometer. The CL signal was detected using the Oxford Instruments MonoCL2 system in Philips XL30 SEM at the electron energy in the beam of 15 keV. The spectra were measured at room temperature.

The PL properties of ZnO films depend on the substrate temperature at film deposition and Cu doping level. For the ZnO films deposited at the low temperature of substrate (T_s = 150 °C), the luminescence was not observed, which is related to the low crystal perfection of the films and a high concentration of non-radiative recombination centers in them [47]. These films were specially selected with account of the annealing-doping effect pronounces greatly. Emission becomes observable after doping and annealing of the films. The normalized PL spectra of the ZnO⟨Cu⟩ films at low, mediate and high levels of doping are shown in Figs. 17a and 17b as well as the reference one (Fig. 17a, curve *1*). The PL spectrum of each film was normalized to the maximal value of the intensity in it. The spectra were normalized in order to present them in one figure, because PL intensities of these films are significantly different.

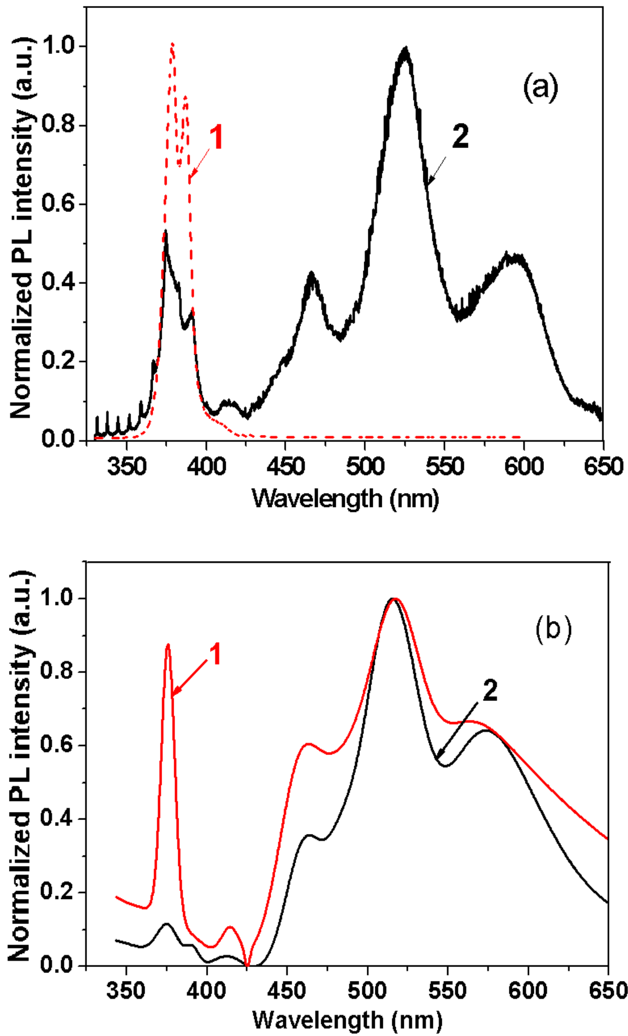

Fig. 17. PL spectra of ZnO films with different concentrations of Cu: a) *1* – reference ZnO film, *2* – mediate concentration of Cu; b) minimum (*1*) and maximum (*2*) Cu concentration.

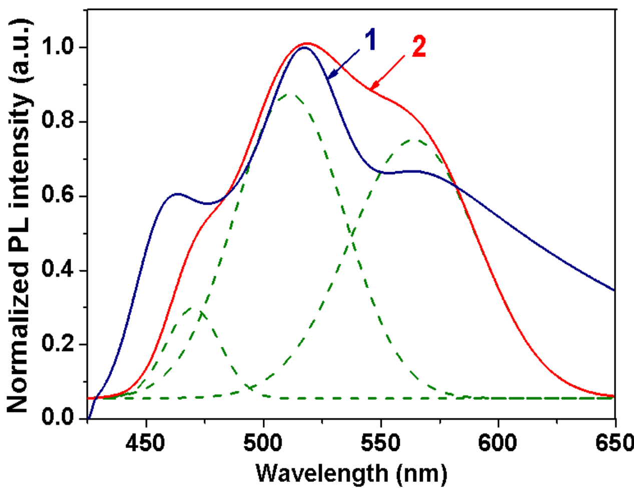

Fig. 18. PL spectra of ZnO⟨Cu⟩ films on silicon (*1*) and sapphire (*2*) substrates at the low level doping. The dashed lines show the results of the Gaussian multipeaks fitting for curve *2*.

After hydrothermal annealing at 600 °C, an intense UV emission of ZnO films occurs. The luminescence spectrum of ZnO film has a narrow peak of UV luminescence at 375 nm with an approximate half-width of 15 nm and the absence of VS emission (Fig. 17a, curve *1*). The significant difference is observed between doped (Fig. 17a, curve *2*) and the reference films spectra (Fig. 17a, curve *1*). After doping with Cu, suppression of UV component is observed and an intense visible spectra emission takes place. It is correlated with results of other authors [41, 48]. The degree of suppression of the UV band is defined by the Cu concentration. The UV band is 10-fold suppressed at high Cu concentration (Fig. 17b, curve *2*). The fine structure in the UV emission band is observed at mediate Cu concentration (Fig. 17a, curve *2*). The energy separation between adjacent peaks is about 72 meV. This value matches well with the longitudinal optical (LO) phonon energy in ZnO. As a rule, phonon replicas have low intensity as compared with that of the UV bands. Thus, in the PL spectra, as a rule, only one to three longitudinal optical phonon features can be distinguished. We observed 6 phonon replicas in the 330…375 nm region of the PL spectrum [42]. As a rule, such a structure is observed in emission of single crystals at the low temperature ~77 K [49]. The presence of phonon structure at ambient temperature suggests that the crystal structure of the films is of high quality. Phonon properties of our ZnO⟨Cu⟩ films with mediate copper concentrations were investigated using the method of Raman scattering [50]. In Raman spectra of the films, authors observed from 6 to 8 phonon repetitions, similar to the bulk ZnO crystal. The presented results also clearly show that ZnO films obtained by the technique applied here possess rather perfect crystal structure which is really close to that of bulk ZnO single crystals [50].

The VS emission consists of the bands with the center at 415, 465, 520, 580…600 nm. The intensity of weak band at 415 nm does not depend on the Cu concentration, and its intensity is very low (~ 5%). The origin of this band is attributed to the intrinsic defects [51, 52]. The VS emission intensity increases with increasing the Cu concentration. The VS emission intensities differ 5-fold for low and high concentrations (Fig. 17b, curves *1* and *2*). The three-peak structure of the VS emission is pronounced most clearly for the mediate concentration of copper (Fig. 17a, curve *2*).

Fig. 18 shows the VS emission spectra of the samples with low-level doping but grown on different substrates – SiN_x/Si (*1*) and α-Al_2O_3 (*2*). At the first sight, the spectra are considerably different. The emission spectrum of ZnO⟨Cu⟩ on Al_2O_3 substrate has a complex shape, and we have resolved them into Gaussian components. We obtained the same three components – blue, green and orange – but with another relationship of their intensities. The difference between these spectra is caused by the difference in the intensity ratios of the constituent bands. The first band is in the blue region with the maximum at 465 nm (2.67 eV). The second and third bands are in the green and orange regions with the maximums at 520 and 580…600 nm, respectively.

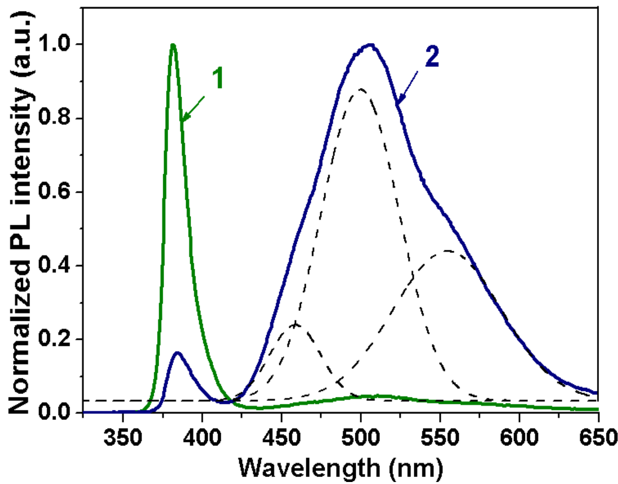

Fig. 19. CL spectra of the ZnO reference film (*1*) and ZnO⟨Cu⟩ film with mediate concentration of Cu (*2*). The dashed lines show the results of the Gaussian multipeaks fitting.

The green band is the most intense. As a consequence, this emission looks like white light. Only green band at 520 nm was observed in the spectrum of ZnO⟨Cu⟩ film grown by EBE. The emission band has the Gauss shape within the temperature range from 4.2 to 300 K.

To determine whether Cu ions penetrate into the depth of the film or they remain mainly on the surface, we investigated the CL spectra of the ZnO⟨Cu⟩ films. It is known that the short-wave light is absorbed at the surface of film, while the electron beam excites the film bulk. The CL spectra of the ZnO (reference) and ZnO⟨Cu⟩ films with the high concentration of Cu are shown in Fig. 19 (curve *1* and *2*, respectively). The CL spectrum of the ZnO film consists of the UV band and a very weak VS emission. The UV band is suppressed significantly, while VS emission is increased in the ZnO⟨Cu⟩ film spectrum similar to their PL spectra. This is evidence of Cu-doping the film bulk.

VS emission of CL demonstrates the three-peak structure similar to VS emission of PL, but positions of the peaks are different. The maximums of emission bands observed upon excitation with the electron beam are shifted to higher energies by 0.1 eV as compared with the band maximums observed under optical excitation. This is caused by different conditions for emission centers formation within the film bulk and near the film surface. Yuldashev *et al.* [53] observed the similar three-band structure of the ZnO film white emission in n-$Zn_{0.9}Mg_{0.1}O$/ZnO/p-$Zn_{0.9}Mg_{0.1}O$ heterojunction structures. It was found that the electroluminescence spectrum of this heterostructure consists of at least three emission bands. The first band is in the blue region with a maximum at 420 nm. The second and third bands are in the green and orange regions with maximums at 505 and 610 nm. The blue emission band is attributed to the radiative recombination of the donor–acceptor pairs (DAP), in which the acceptors are the nitrogen atoms, and this emission band might be originated from radiative recombination in p-$Zn_{0.9}Mg_{0.1}O$. The green emission band is caused by the recombination of DAP, where the deep donors are the vacancies of oxygen, and the orange emission band is attributed to the oxygen interstitials. The latter two emission bands originate from the ZnO active layer. However, our results, which show similarity of the ZnO⟨Cu⟩ film emission spectra on various substrates (see Fig. 18), demonstrate that the luminescence centers might be attributed precisely to the ZnO film and not to its interface or to the substrate as in [54].

The dependence of emission spectra on the doping level of copper (Fig. 17b) indicates that the luminescence centers are the copper ions or complexes, which include copper. It has been shown that the copper doping gives three types of Cu_{Zn} ($3d^9$), Cu_{Zn} ($3d^{10}$) and Cu_i point defects in ZnO [41]. The first two types are the acceptors in two charge states – $3d^9$ and $3d^{10}$ and the third is the donor. The $3d^9$ state is in close proximity to the valence band. Another electron state, $3d^{10}$, lies deeper in the forbidden band of ZnO. At a high concentration of copper impurities, it begins to compensate itself, forming the donor's and acceptor's point defects.

We can assume that the presence of three bands in VS emission is caused by these defects. The reason for this is as follows. The optical depths of the copper acceptor levels relatively to the valence band are 0.1 and 0.38 eV for the two charge states $3d^9$ and $3d^{10}$, respectively. The difference in the emission energy of Cu^+ and Cu^{++} luminescence centers should reach 0.28 eV. This value is in good agreement with the difference of the blue (2.67 eV) and green (2.38 eV) radiation energy of 0.29 eV. The orange band can be attributed to the impurity defects associated with interstitial copper in combination with its own lattice defect acceptors. The introduction of copper into ZnO in the form of three types of defects is a feature of copper doping by thermal diffusion techniques through the film surface. Doping from the target during film growth (EBE) provides luminescence centers of only one type. It follows from the results of hydrothermal annealing of the ZnO films with different copper concentrations obtained by EBE deposition. The emission spectra had only one green band at 520 nm in a wide temperature range from 4.2 up to 300 K.

Attenuation of the UV radiation intensity with introduction of copper may be the result of the deterioration of the film crystal structure or appearance of competitive additional radiative recombination channels. However, the morphological and optical results indicate that the deterioration in crystal structure was not observed. AFM investigation of doped film surface indicates a strongly developed surface with larger grains and nanocrystals in comparison with that of films without doping. The presence of the phonon replicas in the emission spectra indicates high crystal quality of ZnO⟨Cu⟩ films.

3d. Luminescent properties of ZnO⟨Ag⟩ films

Wide band gap semiconductor ZnO (3.4 eV) is considered to be promising material for light emitting devices in the UV spectral region, namely: UV light emitting diodes, blue luminescent devices, and UV lasers [55, 56], because of its low cost and relatively low deposition temperature as well as its optical and electrical properties. The main advantage of this material, especially over well-known GaN, is the extremely high value of the binding energy of free excitons (60 meV), which enhances the energy transfer to luminescence centers. On the other hand, ZnO is a material with high concentration of native defects. These defects, generated during growth process, obstruct obtaining ZnO films of high crystal and optical quality acceptable for optoelectronic applications [55–58].

The properties of zinc oxide depend heavily on the preparation conditions and impurity composition [56]. Doping the films with selective elements could adjust their luminescent characteristics and accelerate the course of their practical applications. Recently, doping effects in ZnO with group-1B elements (such as Cu, Ag, and Au) has attracted great attention. Among the group 1B dopants investigated, Ag was found to be the most favorable activator for enhancing UV emission in ZnO [59, 60]. It had been shown [36, 40] that introduction of Ag into the film bulk improves the crystal structure of the ZnO film, as supported by the increase in the grain size and appearance of an intense UV emission band. Therefore, as the activator for enhancing UV emission in ZnO we used silver.

Thin films of Ag-doped ZnO were prepared by oxidation and Ag doping the ZnS films grown by MOCVD on a glass substrate [40]. Oxidation of ZnS films and Ag doping the ZnO films were carried by CSS method at the temperature < 700 °C. Ag source and glass substrate were separated from each other by ceramic strip spacers of about 1 mm thickness. The annealing atmosphere was prepared by decomposition of oxygen-containing compound. Thin-film structures were additionally annealed after doping in the same atmosphere at the temperature 750 °C for 1 h.

It was found that the Ag-doped films have a higher degree of crystallinity than non-doped ZnO films. AFM micrography showed that the films are grain-like, and the grain size increases with an increase in the Ag loading level. Surface morphology of the annealed ZnO⟨Ag⟩ films is characterized by a distinct hexagonal grain structure. Atomic force microscopy revealed that the films were structured with an average grain size close to 200 nm. Flat-top ZnO⟨Ag⟩ films were obtained with the surface roughness of 7 nm. This value for ZnO films was 120 nm. The samples that show the smallest surface roughness also show strong UV emission at room temperature. There is a large difference between the emission spectra of the as-deposited films, doped films, films after post-treatment. The as-deposited ZnS films are transparent and do not exhibit PL. Luminescence arises after Ag-doping. The emission colour is green. The spectrum consists of one band with the emission maximum at 500 nm. After the annealing treatment, the luminescent properties are changed. The emission color becomes green-blue. The PL intensity increases markedly. Intense emission in the ultraviolet region with the green one in the visible region is observed at room temperature. The spectrum consists of two bands with the emission maximums at 380 and 500 nm. Ultraviolet band contribution is 0.65 of the total. Strong UV emission was observed in ZnO thin films grown by atomic layer epitaxy. It proves high-quality ZnO⟨Ag⟩ films prepared using a simple vacuumless method.

As a rule, doping the ZnO films is accomplished during the growth process, when using magnetron assisted sputtering of the target with the proper composition, or simultaneous electron-beam coevaporation from different sources [41]. As an alternative to the existing methods, in [78] the silver impurity was introduced into the already-deposited polycrystalline ZnO film. Isothermal CSS process [4] has been used for doping ZnO films with Ag under atmospheric pressure. The doped ZnO⟨Ag⟩ films were heated in humid air. The beneficial effect of water vapor on growth of ZnO crystals is well known. At the same time the effect of water vapor annealing on ZnO⟨Ag⟩ films was not investigated in-depth, although there is a mention of the positive effect of such annealing on structural properties of ZnO films [44, 45, 61].

Initial ZnO films (thickness close to 0.5 μm) were deposited by radio-frequency magnetron sputtering of Zn target in a vacuum chamber onto silicon and sapphire substrates at the substrate temperatures T_s = 150 °C and 220 °C. Ag doping the ZnO films was carried out using the CSS process at atmospheric pressure for 1 h at the doping temperature T_d within the range 500…600 °C. The silver block was used as Ag source, the ZnO film/SiN_x buffer layer/Si plate and the ZnO film/α-Al_2O_3 plate were used as substrates. The substrates and Ag source were separated by the 1-mm thick ceramic spacer. Ag was introduced into the ZnO film by using vapor condensation on the film surface and subsequent diffusion into the film bulk when heating in a furnace. This method enables to control the doping element concentration, since there is a correlation between the metal vapor pressure, the concentration of doping element in the film and the CSS doping temperature T_d.

We have found that noticeable changes of luminescence spectra starts at the metal vapor pressure corresponding to the doping temperature T_d = 500 °C. At this temperature, the vapor pressure of silver is $1.33\cdot10^{-6}$ Pa [46]. The maximum temperature was defined as that at which the vapor pressure of silver increases by one order of magnitude. This temperature equals 570 °C, and the pressure of the vapor is $1.33\cdot10^{-5}$ Pa. We used two doping levels. The low level of doping corresponded to $1.33\cdot10^{-6}$ Pa and the high one – to $1.33\cdot10^{-5}$ Pa. The Ag content in the ZnO⟨Ag⟩ films was determined using energy dispersive spectrometer (EDS, JSM-6701F). It was found that the Ag concentration reached 0.03 at.% in the ZnO film doped at 500 °C and 0.3 at.% in the ZnO film doped at 570 °C.

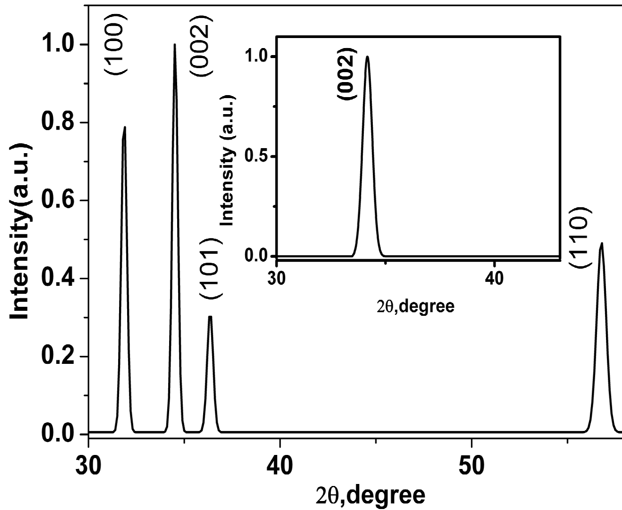

Fig. 20. XRD patterns of ZnO⟨Ag⟩ thin films on the silicon and sapphire (the inset) substrates.

After the CSS processing, ZnO⟨Ag⟩ films were annealed at the temperature T_{an} = 600 °C in wet media for 1 h, water vapor density being close to 0.08 g/m^3. It is known [62] that the weak UV luminescence appears at 77 K in the ZnO films after the long (about 17 hours), high-temperature annealing in air at 800 °C. However, annealing in humid air resulted in appearance of the intense room-temperature UV and VS luminescence even at the lower temperature T_{an} = 600 °C and short 1-h annealing (see curves *1* in Figs 23 and 24). We have used just this type of annealing to determine the nature of the effect of silver doping on the properties of the ZnO films. Beside the ZnO⟨Ag⟩ films, the ZnO reference films were treated at the same conditions in order to separate the effects of the temperature annealing and doping on the properties of films. The PL spectra were recorded using the Horiba JobinYvon T64000 spectrometer. The luminescence was excited by a 337.1 nm pulsed nitrogen laser with 100 Hz pulse repetition rate, 9 ns pulse duration, and 5 kW pulse power, measured at room temperature. Some luminescence spectra were measured at different angles to exclude the influence of interference.

XRD measurements showed that all ZnO films have a polycrystalline hexagonal structure. Fig. 20 presents the XRD patterns of ZnO⟨Ag⟩ films deposited on SiN_x/Si (silicon) and α-Al_2O_3 (sapphire) substrates. In the XRD pattern of the film on silicon substrate, one could observe four diffraction peaks that match well with the (100), (002), (101) and (110) reflections of the hexagonal wurtzite structure of ZnO. Thus, the XRD spectrum is a good reason for the suggestion that the crystalline axis of the grains are randomly oriented in the polycrystalline ZnO film, therefore it has a weak texture. Apparently, such untextured growth of ZnO film was obliged to silicon substrate with amorphous SiN_x layer.

In contrast, ZnO⟨Ag⟩ films on sapphire substrates consist of grains with the preferred (002) orientation (Fig. 20, inset). The *c*-axis is perpendicular to the substrate. The intensity of the peak (002) increases two-fold for films doped with silver on a sapphire substrate in comparison with those on the silicon substrate. Thus, it can be concluded that ZnO films deposited on the sapphire substrate have better crystalline quality as compared to the ZnO films deposited on the silicon substrate. However, the position of 2θ angle 34.37° is somewhat lower than for ZnO powder diffraction standard 34.42° (JCPDS File NO.75-0576 from ASTM). The deviation of the diffraction peak position for our ZnO films from ASTM value (34.42°) is apparently caused by the film stress with compressive components parallel to *c*-axis.

Because introduction of the Ag impurity by CSS method is based on the diffusion of Ag ions into the films through the grain surface or grain boundary, AFM was applied to study surface morphology modification linked to the doping process. The typical AFM images of undoped and Ag-doped ZnO films are shown in Fig. 21. Fig. 21 illustrates the effect of the doping temperature T_d (a, c) and Ag doping (b, d) on morphology of film surface at the different levels of doping. The AFM images show that the films have a grain structure and the average grain size increases with increasing the Ag doping level. All undoped ZnO samples display approximately smooth surfaces with the roughness of 5…8 nm (Table). These films have grains with the mean diameter 40 and 90 nm for T_d = 500 °C and 570 °C, correspondingly. Surface morphology changes noticeably with the Ag doping. Surfaces of the ZnO⟨Ag⟩ films for both T_d temperatures demonstrate grain growth and aggregations of grains (Figs 21b, 21d). The grain size reaches 100 and 160 nm, correspondingly, for low (0.03 at.%) and high (0.3 at.%) doping levels. For these films, the surface roughness (RMSR) reaches 23 and 40 nm (Table). The difference between the highest and lowest points within the given area is 190 and 330 nm (Table).

Table. Morphological parameters for the ZnO⟨Ag⟩ and reference ZnO films on the silicon substrate.

Sample	R_a, nm	RMSR, nm	Z_{range}, nm
ZnO, 500 °C	4.64	5.98	56.60
ZnO⟨Ag⟩, 0.03 at.%; 500 °C	18.38	23.73	191.33
ZnO, 570 °C	5.93	7.61	67.36
ZnO⟨Ag⟩, 0.3 at.%; 570 °C	32.69	40.65	332.37

Deposition temperature T_s = 150 °C, R_a – average arithmetic roughness, RMSR – root mean square roughness, Z_{range} – range of surface heights.

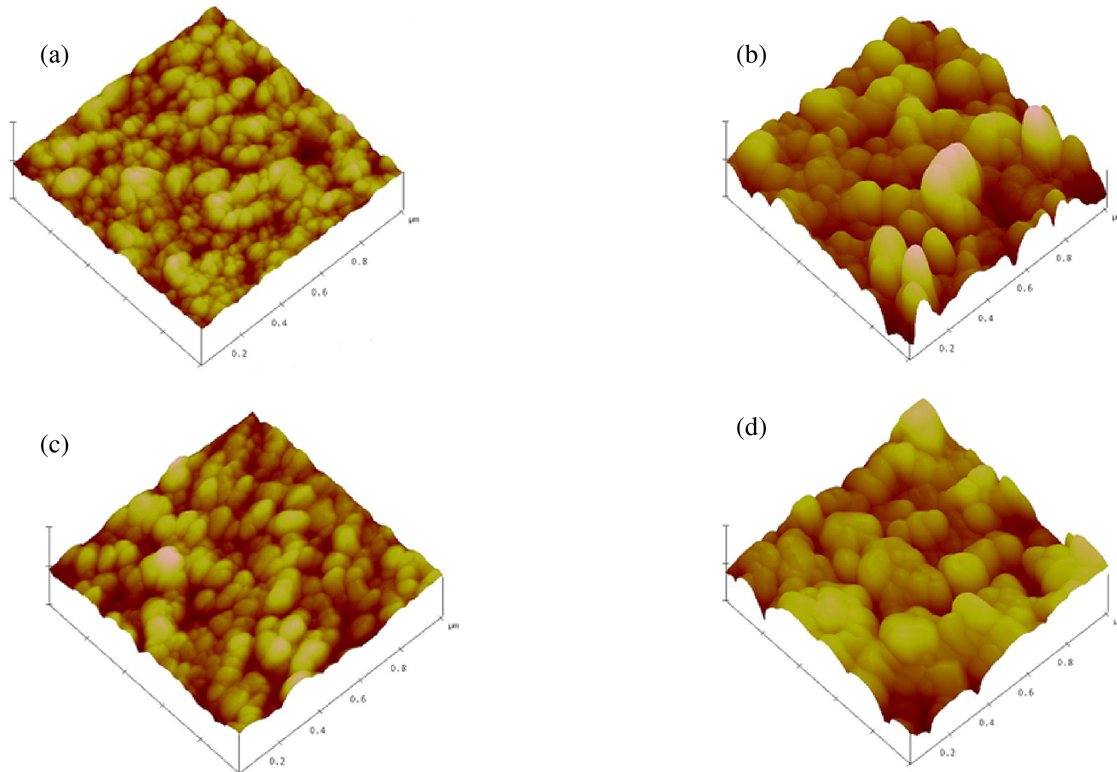

Fig. 21. AFM images of the reference ZnO films (a, c) and Ag-doped ZnO films (b, d). Initial ZnO films were deposited at the substrate temperature T_s = 150 °C. The doping temperature T_d = 500 °C (a, b) and 570 °C (c, d). The Ag doping level 0.03 at.% for (b) and 0.3 at.% for (d). T_{an} = 600 °C in wet medium.

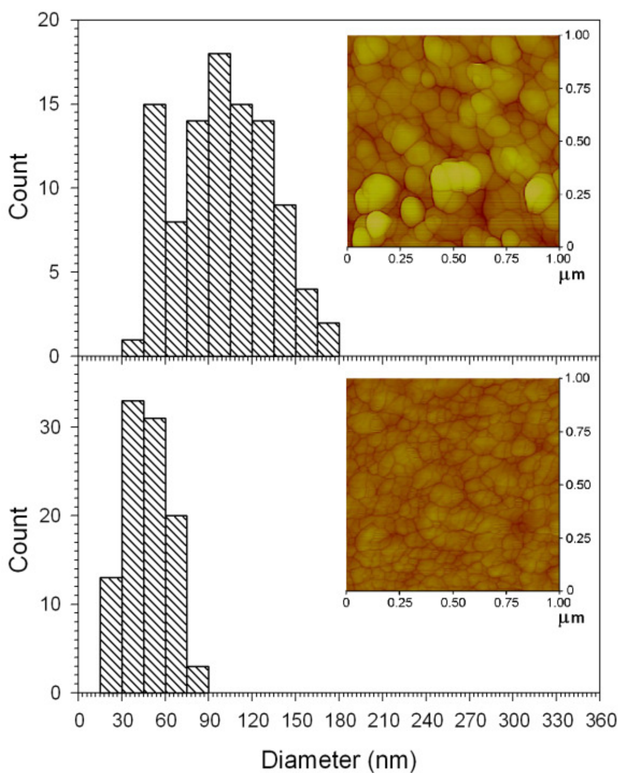

Fig. 22. Grain diameter distributions for ZnO⟨Ag⟩ (a) and reference ZnO (b) films. T_s = 150 °C, T_d = 500 °C, T_{an} = 600 °C in wet medium. The Ag doping level is equal to 0.03 at.%.

From the statistical viewpoint, surface transformation under doping could be illustrated with grain diameter histograms. Grain diameter distributions for ZnO⟨Ag⟩ (Fig. 22a) and reference ZnO (Fig. 22b) films are shown in Fig. 22. Investigation of surface morphology of the ZnO thin films showed that grain size distribution is homogeneous. Significant widening of the surface height takes place for the doped films. The annealing and Ag doping promote increasing the size of grains and modification of grain size distribution (Figs 22a, 22b). As evident from Fig. 22, the distribution view is different at annealing and Ag doping. The latter leads to more inhomogeneous distribution and increases the size of the grains.

The PL properties of the ZnO films depend on the substrate temperature at film deposition and Ag doping level. For the initial ZnO films deposited at the low temperature of substrate ($T_s \leq 220$ °C) the luminescence was not observed. This is caused by the low crystal perfection of films and a high concentration of non-radiative recombination centers in them [47]. Emission becomes observable after the doping and annealing of the films. The normalized PL spectra of the ZnO⟨Ag⟩ films (curves *2*) deposited on different substrates at low and high levels of doping are shown in Figs 23, 24 as well as the reference ones (curves *1*). The PL spectrum of each film was normalized to the maximal value of intensity in order to present them in one figure because the PL intensities inherent to the films are significantly different.

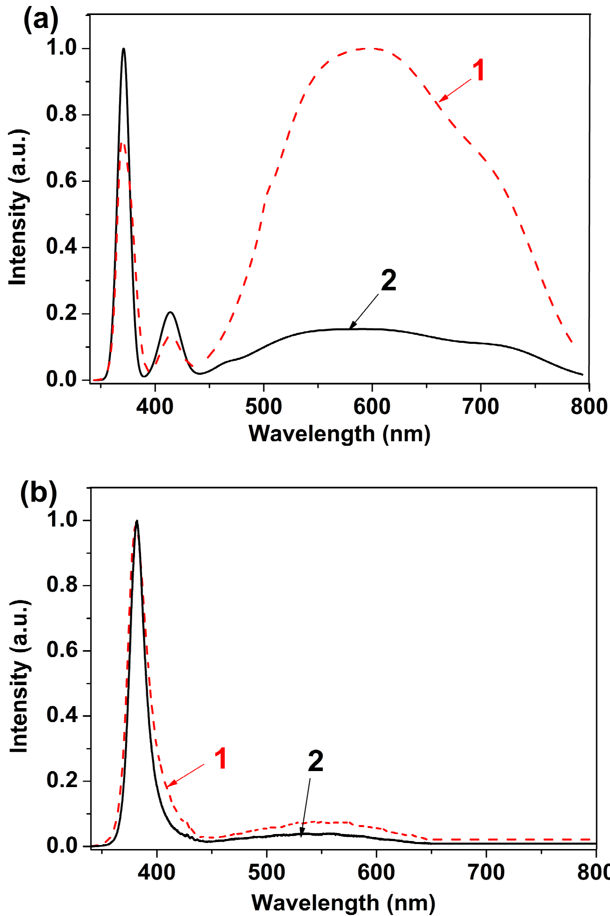

Fig. 23. PL spectra of the ZnO⟨Ag⟩ and reference ZnO films on the sapphire substrate. Initial ZnO films were deposited at the substrate temperature T_s = 150 °C (a) and 220 °C (b). Doping temperature T_d = 500 °C. $T_{an.}$ = 600 °C in wet medium. The concentration of Ag – 0.03 at.%.

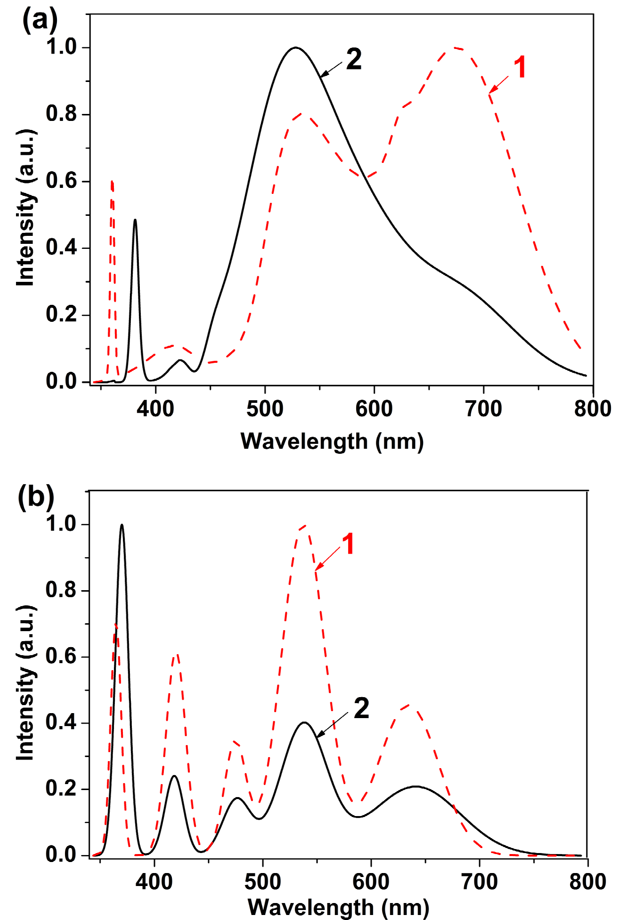

Fig. 24. PL spectra of the reference ZnO and ZnO⟨Ag⟩ films on the silicon substrate. The initial ZnO film was deposited at the substrate temperature T_s = 150 °C. Doping temperature T_d = 500 °C (a) and 570 °C (b). The concentration of Ag – 0.03 at.% (a), 0.3 at.% (b). T_{an} = 600 °C in wet medium.

After hydrothermal annealing at 600 °C, intense emission of the ZnO films appeared. There are several bands in PL spectra: one of them is situated in the UV region, while the others occur in the VS region. UV emission originated from the excitonic recombination corresponding to the near band gap emission of ZnO and therefore indicates good crystallinity of the annealed ZnO films. VS emission is related with defect states.

The emission spectra of the films deposited on the sapphire substrate at 150 and 220 °C are different (Fig. 23). The luminescence spectrum of ZnO film deposited at T_s = 150 °C (Fig. 23a, curve *1*) consists of three bands – at 370, 415 and 600 nm. The 370 and 600 nm bands are similar in their intensity. One of them is narrow and located in UV region, while another is asymmetric broad band in VS region. The spectrum of the film deposited at T_s = 220 °C is characterized by the intense UV band at 380 nm and very weak emission in the VS range at 550 nm (Fig. 23b, curve *1*). The ratio of I_{UV}/I_{VS} is 14. UV emission originates from crystalline ZnO, and VS emission is related with defects. Therefore, the intensity ratio of the UV emission to the VS emission can be a good standard for the quality of the films.

The PL spectra of the reference ZnO films on the silicon substrate consist of UV, V, G, R bands with the centers at 365, 415, 530 and 675 nm, respectively (Fig. 24a, curve *1*). The most intense was red (R) band at 675 nm.

The PL spectra of ZnO films on different substrates have both similarities and differences (see Figs 23a, 24a). The similarity is that luminescence takes place at room temperature and consists of bands with approximately equal intensity in VS and UV spectral regions. The differences are manifested by the different PL intensities and the different positions of PL bands maximums. PL intensity of ZnO films on the sapphire substrate are 20 times that of the films on the silicon substrate. The relative intensities of UV and V bands are approximately (± 10%) equal for two different substrates. The ratio of the intensities of V and UV bands (1:5) does not vary with the type of substrate. At the same time, the low energy bands differ greatly. The B–R emission of ZnO films on sapphire substrate contains broad (440…800 nm) asymmetric band with its peak at 600 nm, whereas that on silicon substrate contains two bands – green (530 nm) and red (675 nm). It is clear that

all these samples have different defect structure, which is reflected in appearance of their defect-related PL spectrum. The difference between defect-related PL spectra on silicon and sapphire substrates may be due to difference in strains between ZnO film and its substrate. Really, the lattice mismatch between ZnO and sapphire is 18% [56]. The mismatch of SiN_x buffer layer between ZnO and Si is (5%).

The differences in the spectra correlate with the difference in the structural properties of the films grown on the crystalline and amorphous substrate – the presence (sapphire) and no texture (Si/SiN_x). The direct band gap of ZnO thin films, at room temperature, strongly depends on preparation technology and crystal structure of samples, covering a wide energy range between 3.25 and 4.06 eV [65–68]. Apparently, changing the position of the maximum of UV band within 3.26…3.4 eV for different samples may be due to that.

With increasing T_d up to 570 °C, broadband VS emission of the reference ZnO film is converted into a well-structured narrow-band emission. The PL spectrum of the reference ZnO film with T_d = 570 °C consists of the bands with the peaks at 365, 420, 475, 535 and 635 nm (Fig. 24b, curve *1*). The most intense is the green band (535 nm). The nature of the observed spectral change indicates a decrease in the number of structural defects and the ordering of film structure, which is related with the increase in grain size (Figs 21a, 21c). The shape of the spectrum is not typical; however, this is not caused by the presence of interference as the film emission spectra were measured under multiple angles. It was found that the positions and intensities of emission bands remained constant. Moreover, there is information about observation of these bands by other researchers. So, for example, the green band (at 535 nm) was observed by H.S. Kang *et al.* [69], the blue (475 nm) and red (635 nm) bands were observed by the authors of [70] and [71], respectively. The green band (at 535 nm) prevails in the spectrum. The intensity of V band (420 nm) is 0.62 of the green band intensity, and 0.9 of the UV band intensity.

Significant difference is observed between the spectra of doped (Figs 23, 24, curves *2*) and reference films (Figs 23, 24, curves *1*). For the ZnO films on the sapphire substrate (T_s = 150 °C), the VS band intensity decreased by an order of magnitude after doping. At the same time, the intensity of the UV band grew markedly. The UV band became the most intense in the spectrum. The intensity of the violet band at 420 nm increased approximately by half. The intensity ratio of I_{UV}/I_{VS} is equal to 10. For the ZnO film deposited at T_s = 220 °C on the sapphire substrate, the silver doping (0.03 at.%) caused the 15-fold increase in the UV band intensity and the 2-fold drop in the intensity of VS emission. The intensity ratio of I_{UV}/I_{VS} increased up to 20. The FWHM for the 380-nm band is 14 nm, which is comparable with that of epitaxial ZnO. The data implies high quality of ZnO⟨Ag⟩ films (Fig. 23b, curve *2*).

Fig. 24 (curves *2*) shows the PL spectra of the ZnO⟨Ag⟩ films with low and high levels of doping obtained by Ag-doping the ZnO films grown on the silicon substrate at T_s = 150 °C. In this figure, the PL spectra of the reference ZnO films are also presented (curves *1*). Upon doping at 0.03 at.% Ag, the change in PL spectrum of the ZnO film is characterized by suppression of the red band (675 nm) (Fig. 24a, curve *2*). The most intense was the green band (530 nm). The maximum of the UV band is shifted (380 nm). The total emission intensity is 4-fold increased. After doping at 0.3 at.% Ag, the maximum of the UV band is slightly shifted (370 nm) and the maximums of the VS bands do not change their positions. The VS bands intensities decreased approximately 3 times, the intensity of the UV band grew markedly. The total emission intensity was 7-fold increased.

Thus, the effect of Ag doping was obvious and identical for all the films, namely, the wide VS bands of PL spectra are suppressed by Ag doping. The intensity of the UV band increases as compared to their reference films.

To determine whether Ag ions penetrate into the depth of the film or remain mainly on the surface, we studied the CL spectra of the ZnO⟨Ag⟩ films. Fig. 25 presents the CL spectra for the ZnO reference film and the ZnO⟨Ag⟩ film with the low concentration of Ag (curve *1* and *2*, respectively). These films were obtained by the processing of the initial ZnO films grown on sapphire substrate at 150 °C. The CL spectra of both ZnO films are almost identical. They consist of two bands at 400 and 525 nm, the UV band is absent. The PL spectra of these films are shown in Fig. 23a.

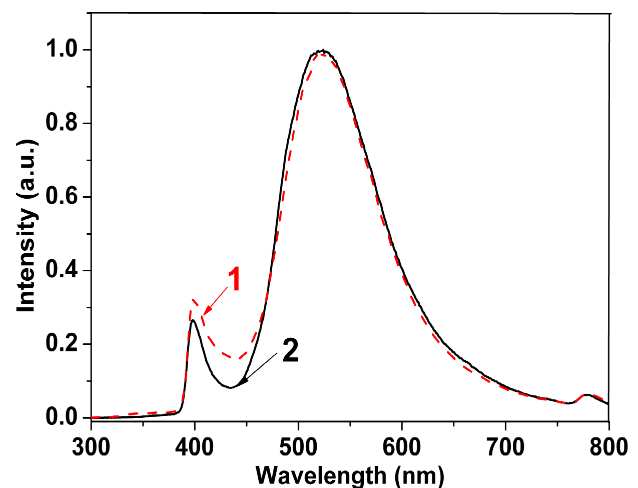

Fig. 25. CL spectra of the reference ZnO film (*1*) and ZnO⟨Ag⟩ film (*2*) with 0.03 at.% Ag. Initial ZnO film was deposited on the sapphire substrate at T_s = 150 °C. T_d = 500 °C. $T_{an.}$ = 600 °C in wet medium.

The V band is present in both cases. This indicates that the V band is not only associated with surface states of the films, but is inherent in the entire bulk of the film.

Comparison of Figs 23a and 25 shows the essential difference between the CL and PL spectra of the ZnO and ZnO⟨Ag⟩ films. The difference in the spectra of PL and CL testify to the heterogeneity of the films. This means that the surface and bulk of films have different defect structures. The similarity of the CL spectra of ZnO and ZnO⟨Ag⟩ films shows that Ag does not penetrate into the ZnO film and remains on the surface. It is probably related with the large ionic radius of Ag (0.113 nm) [35]. Since the ionic radius of Cu is much smaller (0.074 nm) [35], it enables to dope ZnO film with copper throughout its entire depth. Really, for ZnO⟨Cu⟩ films, the PL and CL spectra were similar [42]. Also, this assumption is confirmed by the results of structural studies of ZnO and ZnO⟨Ag⟩ films.

Comparative analysis of the XRD patterns of the Ag-doped and undoped ZnO films has revealed no difference in peak positions and FWHM for the whole diffraction spectrum and for both types of substrates. However, if we assume that Ag occupies interstitial positions or replaces Zn in the cation sublattice of ZnO, it would cause a change in the value of periods of the crystalline lattice (or peak positions), because the Ag^+ radius (0.113 nm) is substantially higher than that of Zn^{2+} (0.074 nm) [35]. Also, no evidences of the second phase of Ag are indicated. Therefore, it is supposed that Ag could be allocated in amorphous surrounding such as grain boundaries or surface of the films; hence its presence can not be detected by X-rays.

Comparison and analysis of the PL emission spectra of Ag-doped and undoped ZnO films allow us to define peculiarities of interaction of silver with the basic matrix. The change of the spectral composition of emission inherent to ZnO films for silver doping at low concentrations indicates silver interaction with centers responsible for this emission (see Fig. 24a). Silver does not exhibit simple acceptor behavior in ZnO, existing mainly as incorporated in complexes with other defects or as Ag–Ag pairs or clusters of several Ag atoms [72]. It is assumed that a slight part of Ag impurity introduced into the crystalline lattice by thermal CSS process passivates some amount of native defects in ZnO. As a result, we have observed the decrease of defect related luminescence and enhancing band-to-band transitions (*i.e.*, excitonic emission).

Other characteristic change of spectra is observed with increasing the concentration of silver by the order of magnitude (up to 0.3 at.%). Spectral composition of VS emission does not change, the contribution of the UV band grows (see Fig. 24b). It means that excess silver does not contact the centers of a luminescence, and drops out on the boundaries of grains, assisting an increase of their size and improvement of crystal structure. It is shown [72] that saturation of the incorporation corresponds to the concentration of 0.05 mol.% of silver, the excess Ag ions would crystallize in the form of metallic silver, which is preferred to loading on the surface of ZnO microrods.

It is clear that all the presented samples have various defects generated during the growth or treatment that is reflected in the visible defect-related PL spectra. Effect of Ag doping is obvious. The UV line intensity increases as compared to that of reference films. The wide bands in the visible range of PL spectrum are suppressed by Ag doping. This suppression of visible emission via Ag doping has been observed in other studies [34, 40, 73-76].

Increasing UV luminescence of ZnO films doped with Ag as compared with undoped ZnO films was noticed earlier [41, 60]. Some authors relate this effect to resonance interaction of the ZnO with surface plasmonic oscillations of Ag nanoparticles [59, 60, 77]. But in our case silver nanoparticles are not observed. Chai *et al.* [77] supposed that Ag may form acceptor levels Ag^{+1} in the band gap of ZnO, which leads to increasing electron-hole recombination and donor-acceptor pairs' emission. Thus, the intensity of the near band emission increases. We found another explanation for increasing of UV luminescence in the ZnO⟨Ag⟩ films [78]. It is seen from AFM images (Fig. 21) that introduction of Ag into the ZnO film results in increasing the ZnO grains. It means that the surface-to-volume ratio becomes lower resulting in domination of excitonic emission above the defect-related one.

It is known that temporal characteristics of the band-to-band and defect emission differ substantially. In the first case, they are characterized by short buildup times, in the second case, they are characterized by longer buildup times. Accordingly, we have carried out research of spectra in the signal registration mode in the short time interval after excitation [79]. Time-resolved luminescence spectra were studied using the method of pulsed spectroscopy [63, 64]. The spectra were recorded using a 0.1-ns gating system. The luminescence spectra were detected at the initial moment after excitation at the leading edge of the laser pulse (at negative value of time delay $t_d = -4$ ns relatively to the laser pulse maximum). The sample excitation duration was equal to 0.7 ns (exciton lifetime).

The time-resolved PL spectra of the ZnO⟨Ag⟩ (curves *1*, *2*) on different substrates and reference ZnO films (curve *3*) are shown in Fig. 26. The PL spectra of the same samples in the stationary mode are shown in Figs 23a, 24b. Comparison of the spectra shows the essential differences between stationary and time-resolved luminescence spectra of ZnO and ZnO⟨Ag⟩ films. The time-resolved PL spectra consist of two narrow bands only: V (415 nm) and UV (370 nm). Any emission in the 450…800 nm region is completely absent. This is an indication of the different nature of high-energy radiation centers bands (UV, V) and the low-energy radiation ones.

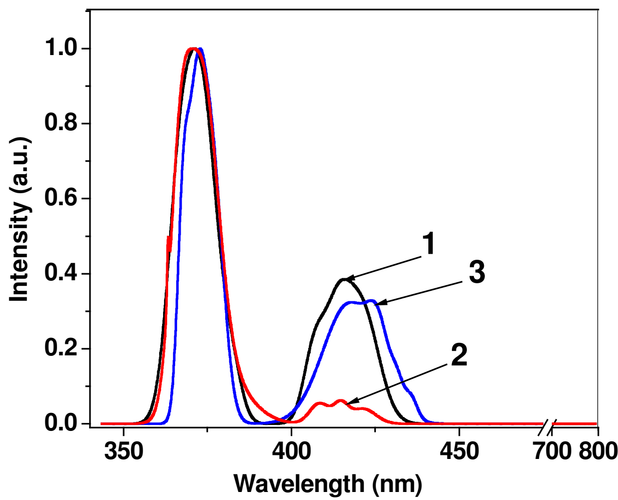

Fig. 26. Time-resolved PL spectra of the ZnO⟨Ag⟩ (*1*, *3*) and reference ZnO (*2*) films on different substrates. The duration of excitation was equal to 0.7 ns for time delays t_d = –4 ns. The sapphire substrate (*1*, *2*), the silicon substrate (*3*). The concentration of Ag is 0.03 at.% (*1*) and 0.3 at.% (*3*).

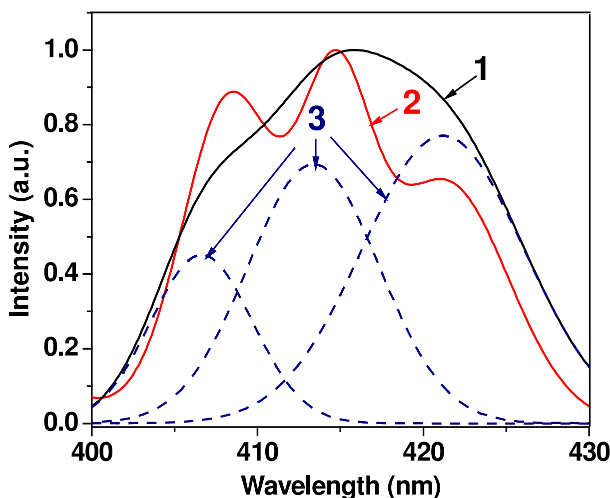

Fig. 27. The detailed view of the V band in the time-resolved PL spectra of the ZnO⟨Ag⟩ (*1*) and reference ZnO (*2*) films on the sapphire substrate. The duration of excitation equals 0.7 ns for time delays t_d = –4 ns. Doping temperature T_d = 500 °C. The concentration of Ag 0.03 at.%. The dashed lines (*3*) show the results of the Gaussian multipeaks fitting for the ZnO⟨Ag⟩ film (*1*).

Fig. 27 demonstrates the detailed view of the V band in the time-resolved PL spectra of ZnO⟨Ag⟩ and the reference ZnO film. The V band of each film was normalized to the maximal value of intensity in order to present them in one figure, because PL intensities for the films are significantly different. The V band of the ZnO⟨Ag⟩ film (*1*) and ZnO film (*3*) are quite different at first glance. It is clearly seen that, in the ZnO film, the V band consists of three sub-bands centred at 408.4, 414.4, 421.3 nm, whereas the V band emission spectrum of ZnO⟨Ag⟩ film has complex shape. Nevertheless, the fitting of the spectra by Gaussian components reveals three components with the same positions of maxima both in ZnO and ZnO⟨Ag⟩ film, but with other relationship of intensities. The components are shown in Fig. 27 only for the ZnO⟨Ag⟩ film (curves *3*). Thus, the difference between these spectra is due to the difference in the intensity ratios of the constituent bands. The relative contribution of each of the bands is determined by the technological conditions of film preparation.

Our experimental results show that the presence of V band in PL spectra of the ZnO films does not depend on the substrate type. However, the B–R emission of ZnO film does depend on the substrate type. The differences in the spectra correlate with differences in structural properties of the films grown on crystalline (sapphire) and amorphous (Si/SiN_x) substrate. All these samples have different defect structure, which is reflected in the appearance of their defect-related PL spectrum. It's known that VS emission is due to the defects of ZnO films. In this region, PL intensity of ZnO films on sapphire substrate is 20 times higher than that of films on silicon substrate.

The effect of Ag doping was obvious and identical for all films; namely, the wide B–R bands of PL spectra are suppressed by Ag doping. The intensity of the UV band is increased as compared to that of reference films. Silver doping does not affect the position of the maximum and the shape of V band. The ratio of intensities I_V/I_{UV} is not changing after doping by 0.03 at.% Ag, but it decreases sharply after doping by 0.3 at.% Ag.

There is no common opinion on the nature of V band emission, which is related with the following reasons. The conditions for appearance and formation of V band, as well as the wavelength of its emission (400…426 nm) are essentially different according to the data of various authors; as a result, the models of corresponding emission centres differ. So, for example, since the V band at 426 nm was caused and strongly enhanced by Al doping, it was assumed that V emission should be attributed to the radiative transition from the Al doping atoms energy level to the valence band [80]. The V band at 420 nm has been observed in the absence of the UV band. This band was attributed to radiative defects related to the interface trap existing at the grain boundaries [81]. The level of the interface traps has been found to be about 0.33 eV below the conduction band edge, and, thus, the violet luminescence is probably caused by the radiative transition between this level and the valence band [81]. The violet emission at 410 nm, which has been frequently observed in glass substrates, was attributed to the oxygen dangling bonds on glass surface or the interface between glass substrate and ZnO nanostructures [82, 83]. The emission bands around 401…412 nm are associated with electron transition from the conduction band minimum to the V_{Zn} level [84, 85, 86]. According to the authors of work [87] the emission band at 402 nm is associated with electron transition

from conduction band tail states to valence band tail states. It's quite possible that the bulk emission of our ZnO films (cathodoluminescence) has a similar nature. At the same time, the nature of radiative transitions of the V band for the surface layer of our films is significantly different. This conclusion is based on the following facts:

1. The V band is observed simultaneously with the UV band. The ratio of the intensities of the V and UV bands (1:5) does not vary with the type of substrate.
2. Behavior of V and B–R bands significantly differs depending on the type of substrate and Ag-doping.
3. Lifetime of the V and UV bands is identical (0.7 ns).

We believe that violet emission in PL spectra of the ZnO films is caused by recombination of electron with a deeply trapped hole in some deep acceptor level. This acceptor level most probably is attributed to V_{Zn}^{-}. It follows from the preparation conditions and the difference between energy values of UV band (3.346 eV) and this V band (2.99 eV). The difference is 356 meV that reasonably agrees with the experimental values of acceptor level 338 meV [84]. The energy distance between the subbands is approximately equal to 0.05 eV for both doped and non-doped samples. With account of the fact that the transverse optical (TO) phonon energy is 50 meV [88, 89], it can be assumed that this structure of the V band is due to presence of the TO phonon replicas.

4. Conclusions

It has been shown that doping the ZnO, ZnS thin films with metals can be successfully performed using the modified Close Space Sublimation method. The relation of EL, PL, CL properties of the doped and non-doped films with their crystalline structure has been established. The improvement of the film crystalline quality as the result of doping leads to a change of all types of luminescence spectra, lowering the EL threshold voltage, rise of the EL and PL brightness. It has been revealed that Ga and Cl act not only as co-dopant for improvement of luminescent properties, but also as promotors for collection and secondary recrystallization processes, which facilitate a coarse-grain formation. The evidence has been presented that the ZnS⟨Cu⟩ film EL mechanism is the direct impact excitation (impact ionization) of luminescence centers by hot electrons, and the emission mechanism is an undelayed recombination. The effect of the Cu- and Ag-doping on the film properties is different. After doping with Cu, an intense VS emission appears, and the suppression of UV component is observed. For all the films, the increase of UV emission as well as the suppression of the wide bands in VS region of PL spectrum are observed as a result of Ag-doping. Thus, doping with the Cu and Ag impurities allows to obtain structures with the controlled emission spectrum: ultraviolet emission or emission of different colors – violet, blue, green, orange, white.

References

1. Hideaki A., Masato A., Aimi Y., Hironori K., Yoji A. Preparation of SnS thin films using close space sublimation. *J. Nanoelectron. Optoelectron.* 2017. **12**, No 9. P. 920–924. https://doi.org/10.1166/jno.2017.2156.
2. Shah N.A., Ali A., Aqili A.K.S. and Maqsood A. Physical properties of Ag-doped cadmium telluride thin films fabricated by closed–space sublimation technique. *J. Cryst. Growth.* 2006. **290**, No 2. P. 452–458. https://doi.org/10.1016/j.jcrysgro.2006.01.051.
3. Britt J. and Ferekides C. Thin-film CdS/CdTe solar cell with 15.8% efficiency. *Appl. Phys. Lett*. 1993. **62**, No 22. P. 2851–2852. https://doi.org/10.1063/1.109629.
4. Khomchenko V.S., Rodionov V.E., Tzyrkunov Yu.A. New method of thin films doping. *Proc. 7-th Int. Symp. SID*, 1998, Minsk, Belarus. P. 218–220.
5. Lytvyn O.S., Khomchenko V.S., Kryshtab T.G. *et al.* Structural investigations of annealed ZnS: Cu,Ga film phosphors. *Semiconductor Physics, Quantum Electronics and Optoelectronica*. 2001. **4**, No 1. P. 19–23.
6. Kryshtab T., Khomchenko V.S., Andracha-Adame J.A., Khachatryan V.B., Mazin M.O., Rodionov V.E., Mukhlio M.F. Phase transition in ZnS thin film phosphor. *J. Cryst. Growth.* 2005. **275**, No 1–2. P. e1163–e1169. https://doi.org/10.1016/j.jcrysgro.2004.11.205.
7. Gorelik S.S. *Recrystallization of Metals and Alloys*. M., Metalurgia, 1978 (in Russian).
8. Arterton A., Brightwell J.W., Mason S., Viney I.V.F. Impact of phase concentrations on structure and electroluminescence of ZnS:Cu. *J. Cryst. Growth.* 1992. **117**, No 1. P. 1008–1011. https://doi.org/10.1016/0022-0248(92)90902-U.
9. Kryshtab T., Khomchenko V.S., Andraca-Adame J.A., Rodionov V.E., Khachatryan V.B., Tzyrkunov Yu.A. The influence of doping element on structural and luminescent characteristics of ZnS thin films. *Superlattices Microstruct.* 2006. **40**, No 4–6. P. 651–656. https://doi.org/10.1016/j.spmi.2006.09.001.
10. Khomchenko V., Rodionov V., Lytvyn P. *et al.* Relation of electroluminescence to the crystalline structure in thin film ZnS-Cu,Ga. *Proc. 8-th Intern. Symp. "Advanced Display Technology"*. 1999. P. 123–129.
11. Huang J., Yang Yi., Liu S., Shenl J. Photo-luminescence and electroluminescence of ZnS-Cu nanocrystals in polymeric networks. *Appl. Phys. Lett.* 1997. **70**, No 18. P. 23335–2337. https://doi.org/10.1063/1.118866.
12. Berezhinsky L.I., Khomchenko V.S., Rodionov V.E., Tzyrkunov Yu.A. Investigation of ZnS-Cu as potential emitting layer for TFEL displays. *Extended Abstracts of the 5th Intern. Conf. on the*

Science and Technology of Display Phosphors. USA. 1999. P. 93–97.

13. Svechnikov S.V., Zavyalova L.V., Roshina N.N. Berezhinsky L.I., Khomchenko V.S., Rodionov V.E., Atdaev B.S. Effect of Ga co-doping on luminescence characteristics of ZnS-Cu films. *Abstr. book of the 3-rd Intern. School-Conference "Physical problems in material science of semiconductors"*, 1999, Chernivtsi, Ukraine. P. 197–198.
14. Kryshtab T., Khomchenko V., Lytvyn P., Prokopenko I. Crystalline structure of thin ZnS-Cu films and recrystallization at Ga doping and annealing. *Proc. of the Seventh European Powder Diffraction Conf.* 2000, Barcelona, Spain. P. 25–26.
15. Kryshtab T., Khomchenko V., Lytvyn P., Prokopenko I. Electroluminescence properties and crystalline structure of thin ZnS:Cu,Ga films. *Proc. 3rd Intern. Conf. on Materials for Microelectronics*. 2000, Republic of Ireland. **1**. P. 267–270.
16. Berezhinsky L.I., Khomchenko V.S., Rodionov V.E., Tzyrkunov Yu.A. ZnO-Cu,Ga: new green-emitting film phosphor. *IX Intern. Symp. "Advanced Display Technology", Abstract book*, 2000, Russia. P. 97–98.
17. Vlasenko N.A., Zynio S.A. and Khomchenko V.S. The mechanism of electroluminescence in zinc sulphide thin films. *Proc. Intern. Conf. on Luminescence*, 1966, Budapest. P. 1803–1810.
18. Henish H.K. *Electroluminescence*. Pergamon Press, Oxford–London–New York–Paris, 1962.
19. Khomchenko V.S., Rodionov V.E., Stiles J. Electroluminescence of the ZnS:Cu film with different coactivators. *Proc. 12th Intern. Workshop on Inorganic and Organic Electroluminescence and Intern. Conf. on the Science and Technology of Emissive Displays and Lighting EL*, 2004, Toronto, Canada. P. 244–248.
20. Khomchenko V.S. The electroluminescence mechanism of ZnS:Cu thin films. *Proc. 10th Intern. Workshop on Inorganic and Organic Electroluminescence*, 2000, Japan. P. 69–71.
21. Roberts G.I. and Crowell C.R. Capacitance energy level spectroscopy of deep-lying semiconductor impurities using Schottky barriers. *J. Appl. Phys.* 1970. **41**, No 4. P. 1767–1771. https://doi.org/10.1063/1.1659102.
22. Vlasenko N.A. and Khomchenko V.S. Franz–Keldysh effect in emission of electroluminescent ZnS:Cu,Cl films. *phys. status solidi* (*a*). 1973. **19**, No 2. P. K137–K139. https://doi.org/10.1002/pssa.2210190252.
23. Vlasenko N.A., Kopytko Yu.V. and Khomchenko V.S. Franz–Keldysh effect in emission of electroluminescent films. *Opt. Spectrosc.* 1974. **37**. P. 779–781.
24. Vlasenko N.A., Timashev S.A., Khomchenko V.S., Chumachkova M.M. On field and temperature dependences of the Franz–Keldysh emission band shift of electroluminescent ZnS-Cu,Cl films. *Ukr. Phys. J.* 1975. **20**, No 4. P. 662–666.
25. Kryshtab T.G., Khomchenko V.S., Papusha V.P., Mazin M.O., Tzyrkunov Yu.A. Thin ZnS:Cu,Ga and ZnO:Cu,Ga phosphors. *Thin Solid Films*. 2002. **403–404**. P. 76–80. https://doi.org/10.1016/S0040-6090(01)01535-8.
26. Khomchenko V.S., Rodionov V.E., Papusha V.P. *et al.* Fabrication and cathodoluminescent properties of the ZnO-Cu,Ga film phosphors, *J. SID*. 2003. **11**, No 1. P. 21–24. https://doi.org/10.1889/1.1831710.
27. Kovalenko L.F., Sevastyanov V.V., Khomchenko V.S., Tzyrkunov Yu.A. Creation of the cathodoluminescence structures based on thin film technology. *Tekhnologiya i Konstruirovanie v Elektronnoi Apparature*. 2008. No 6. P. 48–49 (in Russian).
28. *Patent 39999 Ukraine*. B01J 2/00, B22F 9/02, B22F9/16, B42D 15/00. The method of creating film cathodoluminophores. Sevastyanov V.V., Kovalenko L.F., Khomchenko V.S., Tzyrkunov Yu.A., Kolomzarov Yu.V. 10.09.2008; publ. 25.03.2009, Bul. No 6, 2009.
29. Janotti A. and Van de Walle C.G. Fundamentals of zinc oxide as a semiconductor. *Rep. Prog. Phys.* 2009. **72**, No 12. 126501 (29 pp.). http://dx.doi.org/10.1088/0034-4885/72/12/126501.
30. Ding J.J., Ma Y., Chen H.X., Shi X.F., Zhou T.T., Mao L.M. Influence of Al-doping on the structure and optical properties of ZnO films. *Physica B*. 2009. **404**, No 14. P. 2439–2443. https://doi.org/10.1016/j.physb.2009.05.006.
31. Oo W.M.H., Saraf L.F., Engelhard M.H. *et al.* Suppression of conductivity in Mn-doped ZnO thin films. *J. Appl. Phys.* 2009. **105**, No 1. Article No 013715 (4 pp.). https://doi.org/10.1063/1.3063730.
32. Tubtimtae A., Lee M.-W. ZnO nanorods on undoped and indium-doped ZnO thin films as a TCO layer on nonconductive glass for dye-sensitized solar cells. *Superlattices Microstruct.* 2012. **52**, No 5. P. 987–990. https://doi.org/10.1016/j.spmi.2012.08.002.
33. Kobayashi K., Udaka H., Matsushima N.S., Okada G. Mechanism of photoinduced charge transfer of Cu-doped ZnO film in strong electric field. *Jpn. J. Appl. Phys.* 1993. **32**, Part 1, No 9A. P. 3854–3859. https://doi.org/10.1143/JJAP.32.3854.
34. Gruzintsev A.N., Volkov V.T., Yakimov E.E. Photoelectrical properties of ZnO films doped with Cu and Ag acceptor impurities. *Semiconductors*. 2003. **37**, No 3. P. 259–262. https://doi.org/10.1134/1.1561514.
35. Lide D.R. *CRC Handbook of Chemistry and Physics.* CRC Press Inc., London, 1994.
36. Kryshtab T.G., Khomchenko V.S., Khachatryan V.B. *et al.* Effect of doping on properties of ZnO:Cu and ZnO:Ag thin films. *J. Mater Sci:*

Mater. Electron. 2007. **18**, No 11. P. 1115–1118. https://doi.org/10.1007/s10854-007-9256-y.

37. Liu H., Yang. J., Hua Z., Zhang Y., Yang I., Xiao I., Xie Z. The structure and magnetic properties of Cu-doped ZnO prepared by sol-gel method. *Appl. Surf. Sci.* 2010. **256**, No 13. P. 4162–4167. https://doi.org/10.1016/j.apsusc.2010.01.118.
38. CraciumV., Elders J., Gardeniers J., Boyd I.W. Characteristics of high quality ZnO thin films deposited by pulsed laser deposition. *Appl. Phys. Lett.* **65**, No 23. P. 2963–2969. https://doi.org/10.1063/1.112478.
39. Ievtushenko A., Karpyna V., Lashkarev G. *et al*. Multilayered ZnO films of improved quality deposited by magnetron sputtering. *Acta Phys. Pol. A*. 2008. **114**, No. 5. P. 1131–1137. https://doi.org/10.12693/APhysPolA.114.1131.
40. Khomchenko V.S., Kryshtab T.G., Savin A.K. *et al.* Fabrication and properties of ZnO:Cu and ZnO:Ag thin films. *Superlattices Microstruct*. 2007. **42**, No 1–6. P. 94–98. https://doi.org/10.1016/j.spmi.2007.04.016.
41. Gruzintsev A.N., Volkov V.T., Khodos I.I., Nikiphorova T.V., Koval'chuk M.N. Luminescent properties of ZnO films doped with group-IB acceptors. *Russ. Microelectron.* 2002. **31**, No 3. P. 200–205. https://doi.org/10.1023/A:1015467204997.
42. Khomchenko V.S., Lytvyn O.S., Mazin M.A., Vlaskina S.I., Rodionov V.E., Demydiuk P.V., Yuldashev S.U. White light emission of ZnO-Cu nano-films. *Nanoscience and Nanoengineering*. 2016. **4**, No 2. P. 46–51. https://doi.org/10.13189/nn.2016.040203.
43. Kryshtab T., Khomchenko V., Martínez Juárez J., Juárez Díaz G. Effect of doping on properties of ZnO-ZnS thin films prepared by oxidation of ZnS films in air and water vapor. *Abstr. book of XVII Int. Mater. Research Congress*, 2008, Cancún, México, 17–21 August 2008, Symposium 4, P. 59–60.
44. Chen X., Ng A.M.C., Djurišić A.B., Ling C.C., Chan W.K. Hydrothermal treatment of ZnO nanostructures. *Thin Solid Films*. 2012. **520**. P. 2656–2662. https://doi.org/10.1016/j.tsf.2011.11.019.
45. Lupan O., Pauporte T., Tiginyanu I.M. *et al.* Comparative study of hydrothermal treatment and thermal annealing effects on properties of electrodeposited micro-columnar ZnO thin films. *Thin Solid Films*. 2011. **519**, No 22. P. 7738–7749. https://doi.org/10.1016/j.tsf.2011.05.072.
46. Hotra Z.Yu. *The Handbook on Technology of Microelectronic Devices*. Kamenyar, Lviv, 1986 (in Russian).
47. Lashkarev G.V., Lazorenko V.I, Evtushenko A.I., Khranovskyy V.D., Blonskyy I.V., Dmitruk I.M., Osmanov T.Sh. Effect of the deposition technology and structure of ZnO films on their photo- and cathodoluminescence. *Ukr. J. Phys.* 2008. **53**, No 9. P. 867–873.
48. Alivov Ja.I., Chukichev M.V., Nikitenko V.A. Green luminescence band of zinc oxide films copper doped by thermal diffusion. *Semiconductors*. 2004. **38**, No 1. P. 31–35. https://doi.org/10.1134/1.1641129.
49. Klingshirn C. ZnO: From basics towards applications. *phys. status solid* (*b*). 2007. **244**, No 9. P. 3027–3073. https://doi.org/10.1002/pssb.200743072.
50. Lashkarev G., Karpyna V., Yaremko A. Multi-phonon excitations textured crystalline films by Raman spectroscopy. *Thin Solid Films*. 2012. **520**, No 21. P. 6499–6502. https://doi.org/10.1016/j.tsf.2012.06.076.
51. Peng X., Xu J., Zang H., Wang B., Wang Z. Structural and PL properties of Cu-doped ZnO films. *J. Lumin*. 2008. **128**, No 3. P. 297–300. https://doi.org/10.1016/j.jlumin.2007.07.016.
52. Lin Gong-Ru and Wang S.-C. Comparison of high-resistivity ZnO films sputtered on different substrates. *Jpn. J. Appl. Phys.* 2002. **41**, Part 2, No 4A. P. L398–L401. https://doi.org/10.1143/JJAP.41.L398.
53. Yuldashev S.U., Nusretov R.A., Khvan I.V., Yalishev V.Sh. and Kang T.W. White light emission from ZnO/$Zn_{0.9}Mg_{0.1}O$ heterostructures grown on Si substrates. *Jpn. J. Appl. Phys.* 2008. **47**, No. 1. P. 133–135. https://doi.org/10.1143/JJAP.47.133.
54. Kayahan E. White light luminescence from annealed thin ZnO deposited porous silicon. *J. Lumin*. 2010. **130**, No7. P 1295–1299. https://doi.org/10.1016/j.jlumin.2010.02.042.
55. Marotti R.E., Giorgi P., Machado G., Dalchiele R.E. Crystallite size dependence of band gap energy for electrodeposited ZnO grown at different temperatures. *Sol. Energy Mater. Sol. Cells*. 2006. **90**, No 15. P. 2356–2361. https://doi.org/10.1016/j.solmat.2006.03.008.
56. Özgür Ü., Alivov Y.U., Liu C. *et al.* A comprehensive review of ZnO materials and devices. *J. Appl. Phys.* 2005. **98**, No 4. Article No 041301 (103 pp.). https://doi.org/10.1063/1.1992666.
57. Zhang S.B., Wei S.H., Zunger A. Intrinsic *n*-type versus *p*-type doping asymmetry and the defect physics of ZnO. *Phys. Rev. B*. 2001. **63**, No 7. Article No 075205 (7 pp.). https://doi.org/10.1103/PhysRevB.63.075205.
58. Janotti A., Van de Walle C.G. Native point defects in ZnO. *Phys. Rev. B*. 2007. **76**, No 16. Article No 165202 (22 pp.). https://doi.org/10.1103/PhysRevB.76.165202.
59. Yan Y., Al-Jassim Y.U., Wei S.-H. Doping of ZnO by group-IB elements. *Appl. Phys. Lett.* 2006. **89**, No 18. P. 181912-1–18912-3. https://doi.org/10.1063/1.2378404.
60. Duan L., Lin B., Zhang W., Zhong S., Fu Z. Enhancement of ultraviolet emissions from ZnO films by Ag doping. *Appl. Phys. Lett.* 2006. **88**,

No 23. P. 232110-1–232110-3. https://doi.org/10.1063/1.2211053.

61. Kryshtab T.G., Khomchenko V.S., Andraca-Adame J.A. *et al.* Luminescence and structure of ZnS-ZnO thin films prepared by oxidation of ZnS films in air and water vapor. *J. Lumin*. 2009. **129**, No 12. P. 1677–1681. https://doi.org/10.1016/j.jlumin.2009.04.069.
62. Baca R., Juárez G., Solache H. *et al.* Luminescence and structural properties of ZnO thin films annealing in air. *IOP Conf. Ser.: Mater. Sci. Eng*. 2010. **8**. P. 012041–012048. https://doi.org/10.1088/1757-899X/8/1/012041.
63. Lakowicz J.R. *Principles of Fluorescence Spectroscopy*. Plenum Press, New York and London, 1983.
64. Piryatinskii Y.P., Yaroshchuk O.V. Photoluminescence of pentyl-cyanobiphenyl in liquid-crystal and solid-crystal states. *Opt. Spectrosc*. 2000. **89**, No 6. P. 860–866. https://doi.org/10.1134/1.1335034.
65. Ko K.-H., Joung Y.-H., Choi W.S, Park M., Lee J., Hwang H.-S. Structural and optical properties of a radio frequency magnetron-sputtered ZnO thin film with different growth angles. *Nanoscale Res. Lett*. 2012. **7**, No 1. Article No 55 (5 pp.). https://doi.org/10.1186/1556-276X-7-55.
66. Tari O., Aronne A., Addonizio W.S., Daliento S., Fanelli E., Pernice P. Sol–gel synthesis of ZnO transparent and conductive films: A critical approach. *Sol. Energy Mater. Sol. Cells*. 2012. **105**. P. 179–186. https://doi.org/10.1016/j.solmat.2012.06.016.
67. Wisz G., Virt I., Sagan P., Potera P., Yavorskyi R. Structural, optical and electrical properties of zinc oxide layers produced by pulsed laser deposition method. *Nanoscale Res. Lett.* 2017. **12**, No 1. Article No 253 (7 pp.). https://doi.org/10.1186/s11671-017-2033.
68. Baxter J.B., Aydil E.S. Epitaxial growth of ZnO nanowires on a- and c-plane sapphire. *J. Cryst. Growth.* 2005. **27**, No 3–4. P.407–411. https://doi.org/10.1016/j.jcrysgro.2004.10.014.
69. Kang H.S., Kang J.S., Kim J.W., Lee S.J., Annealing effect on the property of ultraviolet and green emissions of ZnO thin films. *J. Appl. Phys*. 2004. **95**. No 3. P. 1246–1250. https://doi.org/10.1063/1.1633343.
70. Zeng H.B., Duan G.T., Li Y., Yang S.K., Xu X.X., Cai W.P. Blue luminescence of ZnO nanoparticles based on non-equilibrium processes: defect origins and emission controls. *Adv. Funct. Mater*. 2010. **20**, No 4. P. 9795–9800. https://doi.org/10.1002/adfm.200901884.
71. Krajewski G., Luka G., Wachnicki L. *et al.* Optical and electrical characterization of defects in zinc oxide thin films grown by atomic layer deposition. *Opt. Appl.* 2010. **39**, No 4. P. 865–874.
72. Wahl U., Rita E., Correia J.G, Agne T., Alves E., Soares J.C. Lattice sites of implanted Cu and Ag in ZnO. *Superlattices Microstruct*. 2006. **39**, No 1–4. P. 229–237. https://doi.org/10.1016/j.spmi.2005.08.065.
73. Fan J., Freer K. The roles played by Ag and Al dopants in controlling the electrical-properties of ZnO varistors. *J. Appl. Phys.* 2006. **77**, No 9. P. 4795–4800. https://doi.org/10.1063/1.359398.
74. Zhang Y., Zhang Z., Lin B., Fu Z., Xu J. Effects of Ag doping on the photoluminescence of ZnO films grown on Si substrates. *J. Phys. Chem. B*. 2005. **109**, No 41. P. 19200–19203. https://doi.org/10.1021/jp0538058.
75. Ahn B.D., Kang H.S., Kim J.S., Kim G.H., Chang H.W., Lee S.Y. Synthesis and analysis of Ag-doped ZnO. *J. Appl. Phys.* 2006. **100**, No 9. Article No 093701 (7 pp.). https://doi.org/10.1063/1.2364041.
76. You J.B., Zhang X.W., Fan Y.M., Yin Z.G, Cai P.F., Chen N.F. Effects of the morphology of ZnO/Ag interface on the surface-plasmon enhanced emission of ZnO films. *J. Phys D: Appl. Phys*. 2008. **41**, No 20. Article No 205101 (4 pp.). https://doi.org /10.1088/0022-3727/41/20/205101.
77. Chai J., Mendelsberg R.J., Reeves R.J. *et al.* Identification of a deep acceptor level in ZnO due to silver doping. *J. Electron. Mater.* 2010. **39**, No 5. P. 577–583. https://doi.org/10.1007/s11664-009-1025-7.
78. Khomchenko V., Mazin M., Sopinskyy M., Lytvyn O., Dan'ko V., Piryatinskii Yu., Demydiuk P. Preparation, structural and luminescent properties of nanocrystalline ZnO films doped Ag by close space sublimation method. *Appl. Nanosci.* 2019. **9**, No 5. P. 623–630. https://doi.org/10.1007/s13204-018-0796-7.
79. Khomchenko V., Sopinskyy M., Mazin M., Dan'ko V., Lytvyn O., Piryatinskii Yu. The violet luminescence band in ZnO and ZnO-Ag thin films. *J. Lumin*. 2019. **213**. P. 519–524. https://doi.org/10.1016/j.jlumin.2019.04.045.
80. Shi S., Wang P., Cui J. and Sun Z. Microstructure and doping/temperature-dependent photoluminescence of ZnO nanospears array prepared by hydrothermal method. *Nanoscale Res. Lett.* 2018. **13**, No 1. Article No 223 (8 pp.). https://doi.org/10.1186/s11671-018-2622-2.
81. Jin B.J., Im S., Lee S.Y. Violet and UV luminescence emitted from ZnO thin films grown on sapphire by pulsed laser deposition. *Thin Solid Films.* 2018. **366**, No 1–2. P. 107–110. https://doi.org/10.1016/S0040-6090(00)00746-X.
82. Teng X.M., Fan H. T., Pan S.S., Ye C., and Li G. H. Photoluminescence of ZnO thin films on Si substrate with and without ITO buffer layer. *J. Phys. D: Appl. Phys.* 2006. **39**, No 3. P. 471–476. https://doi.org/10.1088/0022-3727/39/3/008.

83. Sakurai Y. The 3.1 eV photoluminescence band in oxygen-deficient silica glass. *J. Non-Cryst. Solids*. 2000. **271**, No 3. P. 218–223. https://doi.org/10.1016/S0022-3093(00)00100-9.
84. Gür E., Tüzemen S., Meral K., Onganer Y. Oxygen deficiency effects on recombination life time and photoluminescence characteristics of ZnO films; correlation with crystal structure. *Appl. Phys. A*. 2000. **94**, No 3. P. 549–554. https://doi.org/10.1007/s00339-008-4960-x.
85. Jeong S.H., Kim B.S., Lee B.T. Photoluminescence dependence of ZnO films grown on Si(100) by radio-frequency magnetron sputtering on the growth ambient. *Appl. Phys. Lett.* 2000. **82**, No 16. P. 2625–2627. https://doi.org/10.1063/1.1568543.
86. Venkatesh P.S, Ramakrishnan V., and Jeganathan K. Investigations on the growth of manifold morphologies and optical properties of ZnO nanostructures grown by radio frequency magnetron sputtering. *AIP Adv.* 2013. **3**, No 8. Article No 082133 (11 pp.). https://doi.org/10.1063/1.4820386.
87. Wang Q.P., Zhang D.H., Xue Z.Y., Hao X.T. Violet luminescence emitted from ZnO films deposited on Si substrate by rf magnetron sputtering. *Appl. Surf. Sci.* 2000. **201**, No 1–4. P. 123–128. https://doi.org/10.1016/S0169-4332(02)00570-6.
88. Vinogradov E.A., Mel'nik N.N., Tsurkan A.E. and Kicherman L.V. Raman scattering in ZnO single crystals. *J. Appl. Spectrosc.* 1977. **26**, No 6. P. 764–767.
89. Gomi M., Oohira N., Ozaki K., Koyano M. Photoluminescent and structural properties of precipitated ZnO fine particles. *Jpn. J. Appl. Phys.* 1977. **42**, Part 1. No 2A. P. 481–485. https://doi.org/10.1143/JJAP.42.481.

Authors and CV

V.S. Khomchenko. PhD in Physics and Mathematics, Senior Researcher of the Laboratory of interference lithography at the V. Lashkaryov Institute of Semiconductor Physics, NAS of Ukraine. Her researcher activities include development of new methods for thin films doping and preparation, characterization of films by using electrical, optical, luminescence methods, investigating the mechanism of luminescence and nature of emission centers. She is the author of more than 180 publications.

M.V. Sopinskyy. PhD in Physics and Mathematics, Senior Researcher of the Laboratory of interference lithography at the V. Lashkaryov Institute of Semiconductor Physics, NAS of Ukraine. The area of his scientific interests includes interference lithography, photostimulated processes in thin-film structures. He is the author of more than 120 publications.

V.A. Dan'ko. PhD in Physics and Mathematics, Head of the Laboratory of interference lithography at the V. Lashkaryov Institute of Semiconductor Physics, NAS of Ukraine. His main research activity is in the field of optics of thin films, photostimulated processes in thin-film structures, nanoparticles and nanostructures, interference lithography. He is the author of more than 140 publications, 9 author's certificates and patents.

G.P. Olkhovik. Researcher of the Department of Information-communication Technologies at the V. Lashkaryov Institute of Semiconductor Physics, NAS of Ukraine. His main research activity is in the field of information technologies, automation of scientific experiment. He is the author of more than 20 publications.